Schrock vs Fischer carbenes: A quantum chemical perspective

Joonghee Won[a,b], Hoimin Jung[a,b], Manoj V. Mane[a,b], Joon Heo[a,b], Seongyeon Kwon[a,b], Mu-Hyun Baik[a,b,*]

[a]Department of Chemistry, Korea Advanced Institute of Science and Technology (KAIST), Daejeon, South Korea
[b]Center for Catalytic Hydrocarbon Functionalizations, Institute for Basic Science (IBS), Daejeon, South Korea
*Corresponding author: e-mail address: mbaik2805@kaist.ac.kr

Contents

Abstract

Early and late transition metal-carbon multiple bonds that have been widely used for many catalytic processes, organic transformations, and olefin metathesis reactions are described. Especially, the development of Schrock and Fischer type olefin metathesis catalysts aided by computational studies is discussed, focusing on work that aims at improving the reactivity, stability, and regioselectivity. The intriguing electronic feature and reactivity of a titanium alkylidyne, which leads to many unique transformations of

organic molecules, are summarized. The development of Fischer type olefin metathesis catalysts to control the regioselectivity in cyclopolymerization of diynes with Ru[II]-alkylidene catalysts employing quantum chemical studies is summarized.
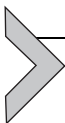
1. Introduction

Transition metal carbene complexes play a pivotal role in organic and inorganic chemistry, where they act as catalysts or key intermediates in various organic transformations, metathesis reactions, asymmetric syntheses, and many catalytic processes.[1,2] The first transition metal carbene complex was introduced by Fischer[3], and it was found that the carbene moiety in these complexes is electrophilic and generally prefers late transition metals in low oxidation states. Named after the original discoverer, the Fischer carbenes often carry stabilizing π-donor substituents such as alkoxy(-OR) or amido(-NR$_2$) groups. Taken together, all these observations suggest that the carbene moiety in Fischer carbenes should be thought of as a neutral ligand that acts as an σ-donor and a π-acceptor. For a little over a decade, this electronic demand was assumed to be generally necessary for carbene functionalities to bind to transition metals. It was therefore a surprise, when Richard R. Schrock prepared a tantalum-based methylene complex[4], in which the carbene proved to be nucleophilic and is bound to high-valent early transition metals. In this case, the carbene is most appropriately thought of as being a dianionic ligand that can act as an σ- and π-donor. These carbenes are now known as the Schrock-carbenes, complementing the Fischer-carbenes. Both classes of carbenes have been investigated intensively over the last five decades and were shown to be highly valuable and versatile for a number of applications. Most notably, transition metal carbene catalysts were shown to promote olefin metathesis reactions, the importance of which was recognized by the Nobel Prize being awarded to Grubbs, Schrock and Chauvin for their pioneering work on olefin metathesis.[5–8]

The electronic structure of metal-carbene fragments is best understood by a donor-acceptor model within the context of the familiar Dewar-Chatt-Duncanson model[9,10] and a schematic representation is shown in Fig. 1A and B. Schrock carbenes have two major orbital interactions between metal and carbene fragments: (i) σ-donation of sp^2-orbital of the carbene carbon and (ii) π-donation of p-orbital of the carbene fragment. Since the carbon fragment can be described as a dianionic ligand, it acts as a nucleophile toward
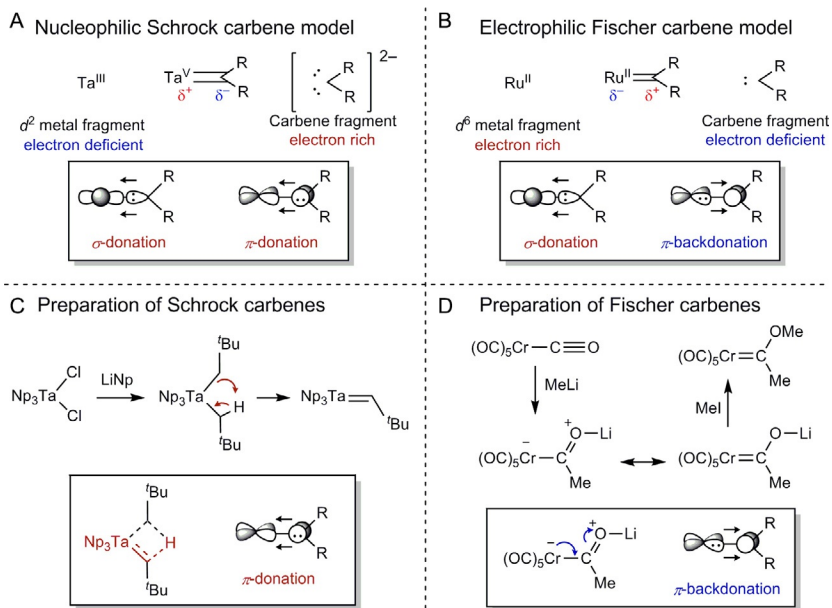
Fig. 1 (A and B) Bonding scheme of Schrock and Fischer type carbene complexes. (C and D) General preparation schemes of each type of carbene species. (Np, neopentyl).

other electrophilic reagents. The carbene fragment is donating two electron pairs, and thus the metal fragment of a Schrock carbene is usually high–valent and electron deficient, possessing empty d-orbitals. In contrast, a Fischer carbene displays a different electronic demand, as described in Fig. 1B: (i) σ-donation of the carbene ligand to the metal center and (ii) π-backdonation from a filled d-orbital to an empty p-orbital of the carbene fragment. Since the carbon of Fischer carbene is holding six valence electrons only, it can be stabilized by electron–rich transition metals *via* π-backdonation.

Typical routes to preparing Fischer and Schrock type carbenes are shown in Fig. 1C and D. For example, a high–valent Ta(V)Cl$_2$ complex can react with two equivalents of neopentyl lithium to first afford a Ta(IV)–dineophentyl complex, which can liberate neopentane by transferring a proton from one neopentyl to another to give the Schrock type neopentylidene complex Np$_3$Ta=CH(^{t}Bu).[11] This deprotonation of the α-proton from one neopentyl ligand by another demonstrates that Schrock carbenes are significantly stabilized by the π-donation from the carbene fragment to the metal as illustrated in Fig. 1A. This finding is also consistent with the general observation that early transition metals with high oxidation states, generally containing 0 to 2 d-electrons, are preferred to form Schrock

carbenes. Fischer carbenes are typically prepared differently. As depicted in Fig. 1D, Fischer carbenes can be prepared from a metal carbonyl compounds, for example, by reacting $Cr(CO)_6$ with MeLi to initially form a zwitterionic complex, which has a resonance structure that contains a $Cr=C$ bond.[12] Treating the adduct with MeI readily affords the Fischer carbene, where the metal-to-ligand π-backdonation plays a key role in stabilizing the electron-deficient carbene fragment. Since metal centers in Fischer-carbene complexes require electrons that can be donated, low oxidation states electron counts close to 18 are preferred.

Over the last two decades, both Fischer- and Schrock-carbenes have been studied by computational methods, which have significantly enriched the fundamental understanding of these important classes of molecules. These quantum chemical studies have been enlightening, since the isolation and characterization of alkylidene complexes proved difficult in many instances. Quantum chemical calculations have been used to elucidate the electronic properties of various intermediates that are thought to be formed during various reactions. Recently, much progress was made in experimentally probing the electronic structure of the metal–carbene bond and understanding their chemical reactivity. These studies will also be highlighted below.

1.1 Early transition metal alkylidenes

The existence of a titanium methylidene as a reactive intermediate was first recognized by Frederick Tebbe in connection with the complex $Cp_2Ti(\mu_2-CH_2)(\mu_2-Cl)Al(CH_3)_2$. Now widely known as Tebbe's reagent, this masked Ti(IV)-methylidene was reported for the first time in 1978[13], but was studied in 1974[14] and is prepared in good yield by addition of excess amounts of $AlMe_3$ to Cp_2TiCl_2 in toluene. In the presence of a mild Lewis base such as pyridine, complex **1** can be activated to give the reactive intermediate, presumably the titanocene-methylidene complex **2** as shown in Scheme 1. Tebbe's reagent facilitates methylene group transfer reactions and can engage in α-hydrogen abstraction. The complex **2** cannot be isolated as a pure compound, but it can be studied and observed in other forms in solution using different types of phosphines to generate complex $Cp_2Ti=CH_2(PR_3)$, at low temperature.[15–18]

The Schrock-carbene complexes attracted notable attention from the quantum chemical modeling community and several computational studies were reported as early as 1984. Employing Hartree-Fock level of theory,
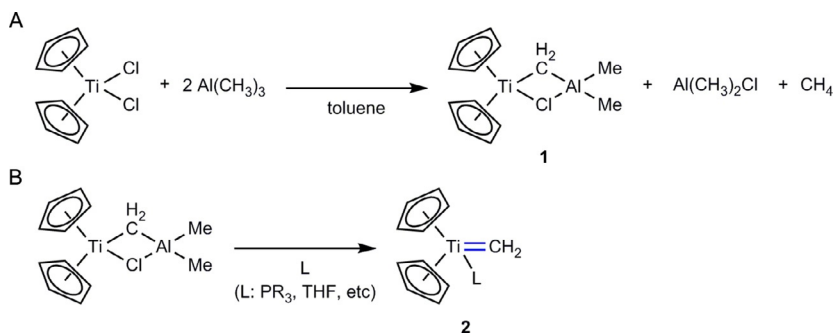
Scheme 1 Synthesis of the titanocene-methylidene complex using Tebbe's reagent. (A) Synthesis of Tebbe's reagent. (B) Observation of titanocene-methylidene aided by phosphines or THF.

Taylor and Hall suggested that the Schrock-carbene complexes $CpCl_2NbCH_2$ and $CpCl_2NbCH(OH)$ exhibit nonclassical behavior distinct from Fischer-carbenes because of the nature of the metal center and not because of any fundamental difference of the carbene ligand.[19] Goddard and coworker analyzed the Fischer and Schrock carbenes employing the generalized valence bond (GVB) method[20] and offered one of the earliest descriptions of the electronic structure of these complexes. The reaction mechanism leading to the formation of the carbenes was also modeled as a decomposition of tetraalkyl titanium, $Ti(CH_3)_4$, to form the product complex $Ti(CH_3)_2=CH_2$. It was found that a bimolecular α-hydrogen abstraction was most likely and preferable over the alternative unimolecular pathway involving an α-hydrogen abstraction by a methyl group to afford methane and the Ti-methylidene.[21] More recent work has made clear that the mechanism of carbene formation is quite complicated and can proceed through different reaction channels. Recent experimental work even implicates a radical coupling pathway[22] that was previously not extensively considered. Interestingly, a well characterized mononuclear titanium methylidene, $(PN)_2Ti=CH_2$ [$PN^- = $ (N-(2-(diisopropylphosphino)-4-methylphenyl)-2,4,6-trimethylanilide)], which is a structural analog of the important Tebbe's reagent was successfully prepared, isolated and structurally characterized. The electronic and molecular structure of the titanium methylidene complex was studied in detail using modern computational methods.[23] The Wiberg bond order[24] between the Ti and C was 1.70 and NBO[25] analysis assigned -0.74 charge to the α-carbon, confirming the general conceptual characterization of the Schrock-carbene in these

modern calculations. The molecular orbital diagram confirms that there are two important electronic interactions, namely, the Ti—C σ-bond interaction (HOMO-11) between the sp-hybridized donor orbital on the $[CH_2]^{2-}$ fragment and the $d_{y^2-z^2}$ orbital of the metal, and the Ti—C π-bonding (HOMO-1) between the lone-pair p-orbital of the $[CH_2]^{2-}$ ligand and a π-acidic d_{yz} orbital of the metal, as illustrated in Fig. 2.

The first example of a zirconium methylidene complex, $Cp_2Zr=CH_2(PPh_2Me)$, was reported by Schwartz over 30 years ago. The unstable nature of the complex made precise structural characterization difficult[26], but recently, several stabilized methylidene complexes of Ti and Zr have been isolated and structurally characterized.[27,28] Notably, few examples of Zr and Hf alkylidene complexes including structural details were reported by Fryzuk.[29–32] The Mindiola group[33] has successfully prepared the
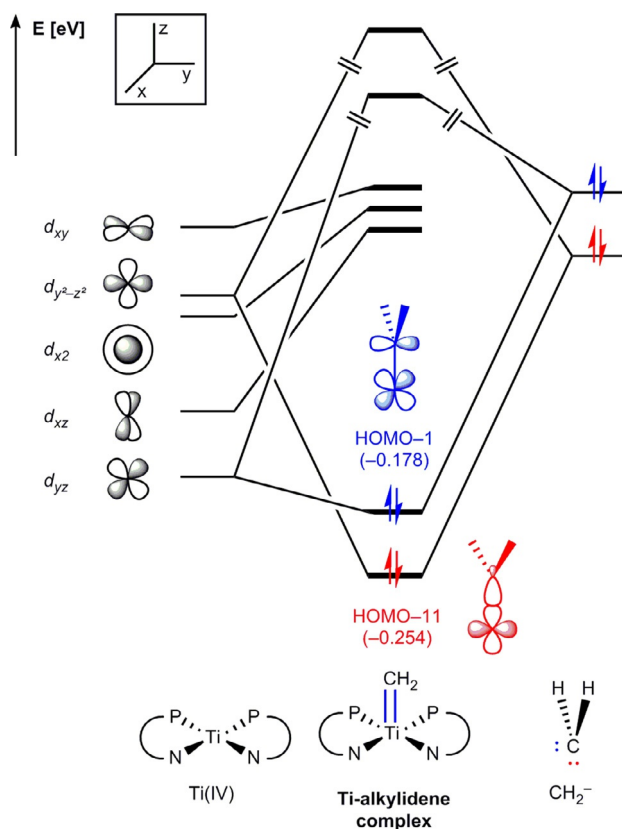

Fig. 2 DFT-calculated qualitative FMO diagram of Ti-methylidene.[23]

dimethyl alkoxide complex of Zr and Hf, (PNP)M(CH$_3$)$_2$(OAr) (M = Zr or Hf), which can give access to the methylidene complex, (PNP)M= CH$_2$(OAr) by photolytically induced α-hydrogen abstraction.

Ozerov[34] reported that the methylidene ligand can be installed on metals utilizing a methyl precursor, (PNP)M(CH$_3$)$_3$ (M = Zr, Hf; PNP$^-$ = N[2-P (CHMe$_2$)$_2$-4-methylphenyl]$_2$). Computational studies clearly showed that the plane defined by the atoms in the [CH$_2$]$^{2-}$ ligand in zirconium alkylidene is perpendicular to the P–Zr–P axis. As shown in Fig. 3, the HOMO derives from the interaction of the filled p_z orbital of the methylidene ligand with the lowest unoccupied d_{yz} orbital of the [(PNP)Zr(OAr)]$^{2+}$ fragment. On the other hand, rotating the [CH$_2$]$^{2-}$ ligand by 90° would enable the interaction of π-bond between p_x and hybridized $d_{xy} + p_x$ orbital of the [(PNP)Zr(OAr)]$^{2+}$ fragment, shown on the left hand side of Fig. 3. Although hybridization of d_{xy} and p_y orbital in [(PNP)Zr(OAr)]$^{2+}$ stabilizes this molecular orbital, the antibonding combination with the nitrogen of PNP and oxygen of alkoxide
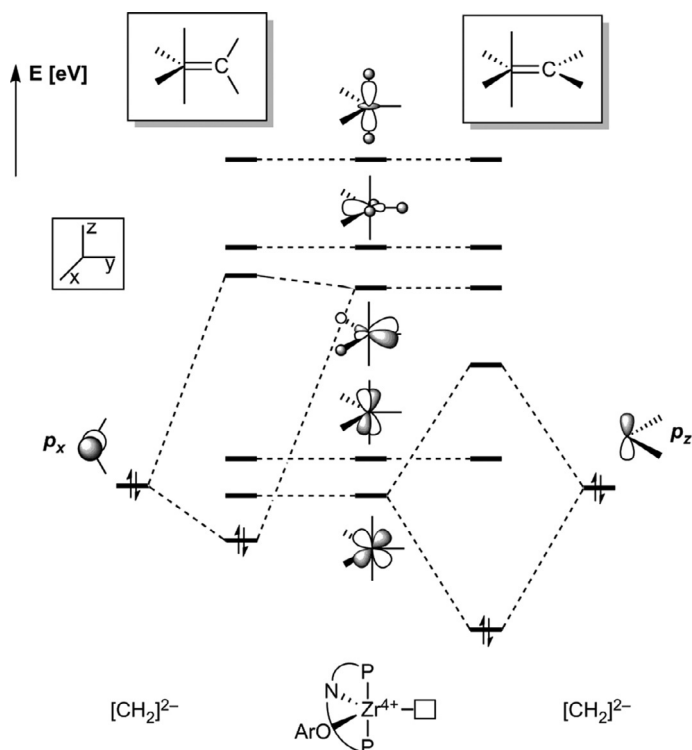

Fig. 3 Molecular orbital diagram for the two plausible conformers of **A** with a differently oriented methylidene unit.[33]

increases the overall energy, hence leading to a HOMO (Zr=C π-bond) that is much higher in energy and a Zr=C π^*-orbital that is also higher in energy. This conceptual MO-diagram offers an intuitively understandable reason for the orientation of the carbene ligand.
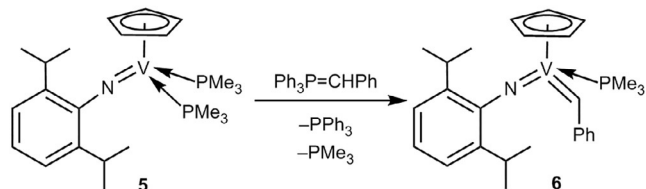
In 1989, Teuben and coworkers prepared the first example of a vanadium(III)-alkylidene complex, CpV(CH^{t}Bu)(dmpe) [dmpe = bis(dimethylphosphino)ethane] (**4**) from the dialkyl precursor **3** by α-hydrogen abstraction as shown in Scheme 2.[35] Later, the first high-valent vanadium(V)-alkylidene complex **6**, CpV(NAr)(CHPh)(PMe$_3$) (Ar = 2,6-(CHMe$_2$)$_2$C$_6$H$_3$) was reported[36], which was prepared from the PMe$_3$-coordinated vanadium(III)-imido complex **5**, CpV(N-2,6-^{i}Pr$_2$C$_6$H$_3$)(PMe$_3$)$_2$, by treating it with Ph$_3$P=CHPh *via* a benzylidene transfer. Recently, Mindiola demonstrated that the series of vanadium(V)-alkylidene complexes can be prepared from vanadium(III) complexes employing π-acids or two-electron oxidants.[37–39] Similarly, four-coordinated cationic vanadium-alkylidene complex **8**, [(nacnac)V(CH^{t}Bu)(THF)][BPh$_4$] (nacnac$^-$ = {(2,6-^{i}Pr$_2$C$_6$H$_3$)-N-C(CH$_3$)}$_2$CH$^-$), was synthesized from a vanadium(III)-dialkyl complex **7**, (nacnac)V(CH$_2^t$Bu)$_2$, by reacting with AgBPh$_4$. Further treatment with MgI$_2$ or I$_2$ gave the neutral alkylidene complex **9** and subsequent alkylation with LiCH$_2$SiMe$_3$ generated the vanadium(IV)-alkyl, alkylidene complex **10**, (nacnac)V(CH^{t}Bu)(CH$_2$SiMe$_3$).[40,41]

Schrock reported the niobium alkylidene Cp$_2$Nb(CHCMe$_3$)Cl, which was prepared by treatment of Nb(CH$_2$CMe$_3$)$_2$Cl$_3$ with 2 equiv. of thallium cyclopentadienide, CpTl. McCamley and coworkers reported the synthesis of the niobium alkylidene by a redox route, in which the one-electron oxidation of Nb(IV)-(η^5-C$_5$H$_4^t$Bu)$_2$(CH$_2$Ph)$_2$ (**11**) along with AgBPh$_4$ produced an unstable benzylidene salt, [Nb(V)(η^5-C$_5$H$_4^t$Bu)$_2$(CHPh)][BPh$_4$] (**12**), which performed C—H activation to generate the cyclometalated product **13** (Scheme 3).[42] Similarly, Otero and coworkers found that oxidizing niobium alkyne complexes can generate a bimetallic vinylidene complex **16**.[43] The synthesis of bimetallic ethylene hydride complexes was also reported.[44] Recently, Mindola and coworkers prepared a rare example of Nb(V)-methylidene complexes, Nb(CH$_2$)(CH$_3$)(CH$_2$PPh$_3$)(OAr″)$_2$ (**18**), by treating NbCl(CH$_3$)$_2$Cl(OAr″)$_2$ with 2 equiv. of NaOAr″ and H$_2$C=PPh$_3$. Thermolysis at 80 °C for 5 days afforded the bridged complex **19**, (Ar″O)$_2$Nb]$_2$(μ_2-Cl)$_2$(μ_2-CH$_2$).[45] Another route to this bridging complex was disclosed to be photoirradiation in benzene using a Xenon lamp. Further reduction gives the methylidyne complex **20**, *via* α-H
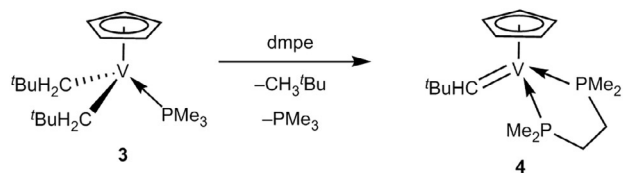
Scheme 2 Selected examples of vanadium alkylidenes through (A) α-H elimination, (B) alkylidene transfer, and (C) oxidatively induced α-H abstraction.
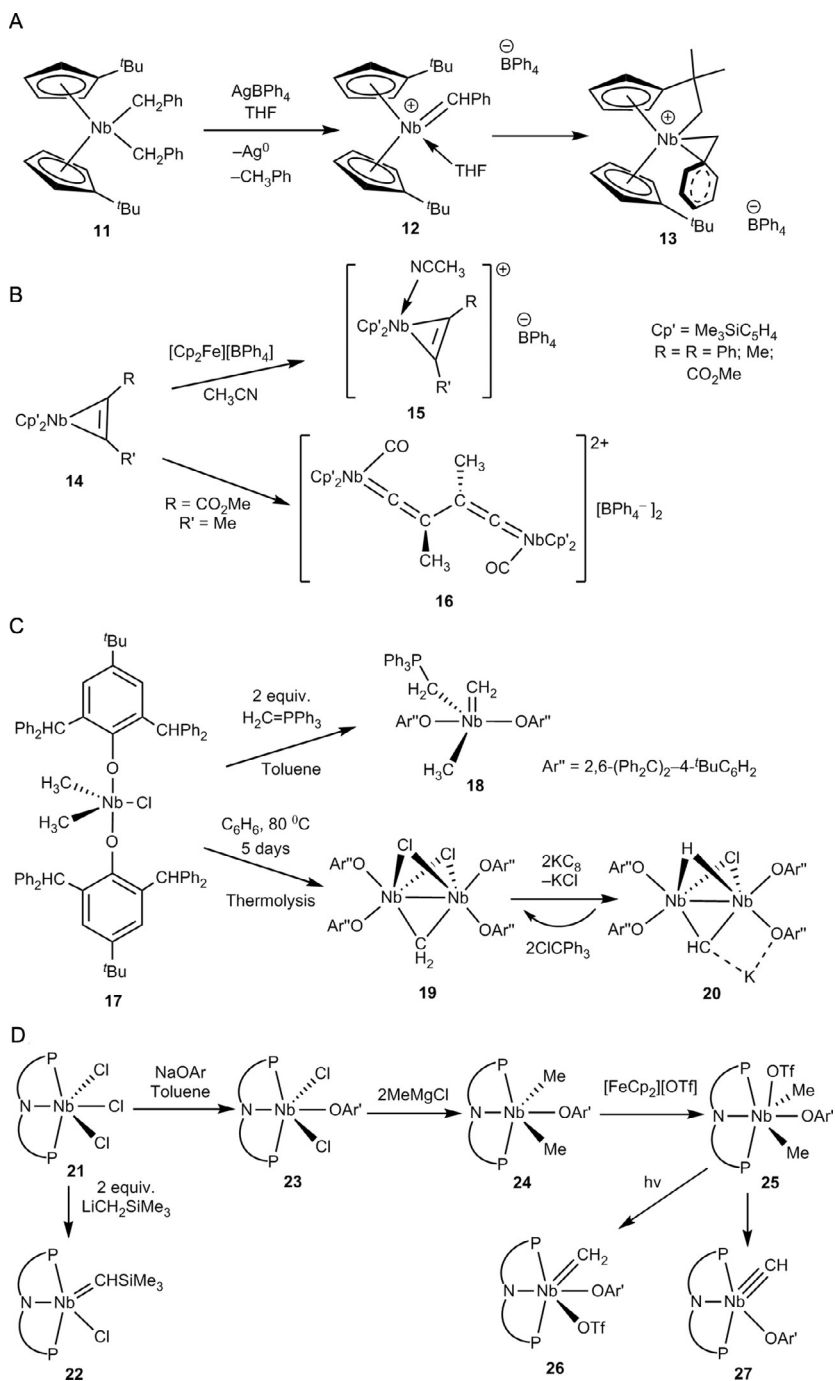
Scheme 3 Synthesis of niobium complexes. (A) Synthesis and reactivity of unstable benzylidene salt **12**. (B) Oxidation of niobium alkyne complex **14** to generate a bimetallic vinylidene complex **16**. (C) Preparation of a rare example of Nb(V)-methylidene complex **18**, and methylidyne complex **20**. (D) Synthesis of Nb(IV) alkylidene **22** and the mononuclear methylidyne complex **27**.

elimination in presence of 2 equiv. of KC_8.[46,47] These advances in preparing these unique complexes are useful and offer a rich foundation for better understanding the structure and bonding of Schrock carbenes.

Pincer type (PNP, ONO) ligands have also been shown to be very useful in stabilizing metal-carbenes. The first paramagnetic Nb(IV) alkylidene **22** was prepared from Nb(IV), (PNP)NbCl$_3$ (**21**) with LiCH$_2$SiMe$_3$. The reaction of **21** with NaOAr$'$ gives the (PNP)NbCl$_2$(OAr$'$) (**23**) complex, followed by the reaction with the 2 equiv. of CH$_3$MgCl that gave the dimethyl complex **24**, (PNP)Nb(CH$_3$)$_2$(OAr$'$). This complex can be further oxidized with [FeCp$_2$] [OTf] and treatment with an phosphorus ylide (H$_2$C=PPh$_3$) produced the mononuclear methylidyne complex **27**, (PNP)Nb(CH)(OAr$'$). The neutral Nb(V)-nitride, (PNP)Nb(N) and terminal alkyne were formed by cross metathesis between the methylidyne complex and RCN (R = ^{t}Bu or 1-adamantyl). Recently, (imido)niobium(V)-alkylidenes, Nb(CHSiMe$_3$) (NR)[OC(CF$_3$)$_3$], containing trianionic ONO ligand was prepared from niobium dialkyl complexes by α-hydrogen elimination, as shown in Scheme 3.[48]

In 1975, Schrock reported the methylidene methyl complex Cp$_2$Ta=CH$_2$(CH$_3$), which was prepared by using [Cp$_2$Ta(CH$_3$)$_2$][BF$_4$] and the ylide H$_2$CP(CH$_3$)$_3$.[4] The other few examples of tantalum-based systems are reported by Rothwell and coworkers, containing the low-coordinate and metastable complex (ArO)$_2$Ta=CH$_2$(CH$_3$) (Ar = (2,6-^{t}Bu$_2$)-4-X-C$_6$H$_2$, X = –H, –OMe).[49,50] The most common approach for forming tantalum methylidene complexes is to use a strong base with the corresponding methyl precursor that is starting with the methyl complex and deprotonating. Rothwell[49,50], Fryzuk[51], Ozerov[52] and Bercaw[53] reported that tantalum methylidene can be accessed by thermally or photolytically promoting α-hydrogen abstraction from the methyl precursors. In the case of Cp*$_2$TaCl(THF) or Cp*$_2$Ta(CH$_3$) the phosphorus ylide H$_2$CP(CH$_3$)$_3$ was employed to generate Cp*$_2$Ta=CH$_2$(Cl) or Cp*$_2$Ta=CH$_2$(CH$_3$) *via* a methylidene transfer, along with the free trimethylphosphine.[54,55] Recently, Mindiola successfully prepared the terminal tantalum methylidene chloride complex **29** (Ar$'$O)$_2$Ta=CH$_2$(Cl)(H$_2$CPPh$_3$) by addition of 2 equiv. of HOAr$'$ to TaCl$_2$(CH$_3$)$_3$ to first form the bis-aryloxide methyl derivative (Ar$'$O)$_2$Ta(CH$_3$)Cl$_2$ (**28**) followed by addition of excess amounts of the ylide H$_2$CPPh$_3$ (Scheme 4).[56]

Carbonyl chromium(0) carbene complex, (CO)$_5$Cr=C(OR)R$'$, was the famous original Fischer type carbene discovered a long time ago as discussed in
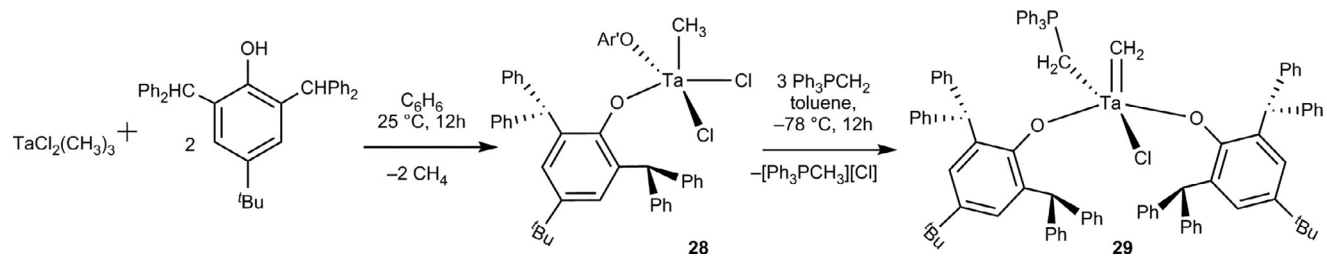
Scheme 4 Synthetic route to tantalum methylidene.
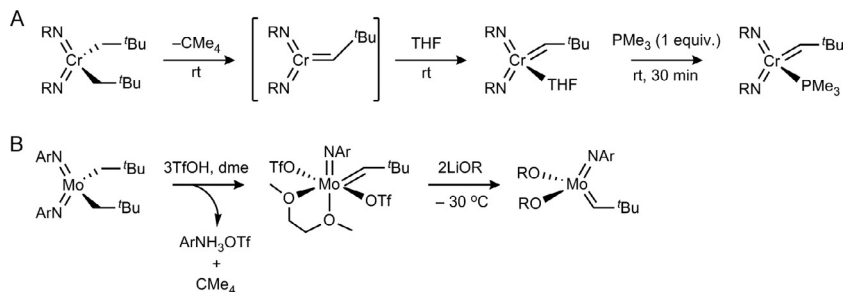
Scheme 5 Synthesis of Schrock type (A) chromium(VI) alkylidene complex and (B) molybdenum(VI) alkylidene complex.

Section 1[57], whereas the first stable high oxidation chromium(VI) alkylidene complex was prepared *via* the α-hydrogen abstraction and the stabilization by phosphine ligand[58] as described in Scheme 5A. One of the Fischer type carbene complexes, $(CO)_5Cr=C(OR)R'$, has been widely used as a carbene precursor for Pd-catalyzed annulation *via* a cycloaddition, which is known as the Dötz reaction[59–61], allowing for constructing highly substituted aromatic rings. In addition, Wang extensively studied the reaction using a chromium(0) Fischer carbene complex that was inspired by palladium-catalyzed self-dimerization of chromium(0) carbene reported by Sierra and coworkers[62], and one of the reactions is described in Scheme 5A.[63,64]

One of the first transition metal carbene complex that was prepared was the tungsten carbonyl carbene, $(CO)_5W=C(OR)R'$ by Fischer and, as described above, the carbene ligand was considered a neutral ligand acting as a σ-donor and π-acceptor. Interestingly, the electronic features of the carbene ligand became notably different compared to previously observed Fischer type carbenes depending on the other ligands, and molybdenum and tungsten carbene complexes that are now thought of being Schrock type $M=C$ bond have been developed extensively, especially for olefin metathesis catalysis. Molybdenum or tungsten imido alkylidene complexes of the type $M(CHR)(NR')(OR'')_2$ (M = Mo, W) are generally prepared *via* the sequence of reactions shown in Scheme 5B.[65] Because of the intense interest in the olefin metathesis reaction for constructing carbon–carbon bonds, theoretical studies of Mo- and W-carbene catalysts have been carried out as early as 1992 and have continued to attract much attention.[66–69] The key results are summarized below in greater detail.

In group 7, rhenium carbenes have received much attention as an olefin metathesis catalyst, whereas Mn- or Tc-carbene complexes have received

less attention. Conventionally, the rhenium carbene motif was accessed by the photolysis of $ReO_2(CH_2^tBu)_3$, that gave $ReO_2(CH^tBu)(CH_2^tBu)$ in high yield.[70] Even though both of Re(V) and Re(VII) alkylidene could be prepared, Re(VII)-alkylidene was found to be a particularly active catalyst for olefin metathesis. Generally, the bisalkoxy or alkyl functionalized alkylidyne/alkylidene complexes of rhenium, $Re(C^tBu)(CH^tBu)(OR)_2$ are employed as highly active olefin polymerization catalysts and these compounds display pseudo-tetrahedral geometry.[71] Interestingly, when the rhenium catalysts were immobilized on silica, they showed promising high activity for olefin metathesis compared to the Mo- and W-based homogeneous catalysts.[72–74]

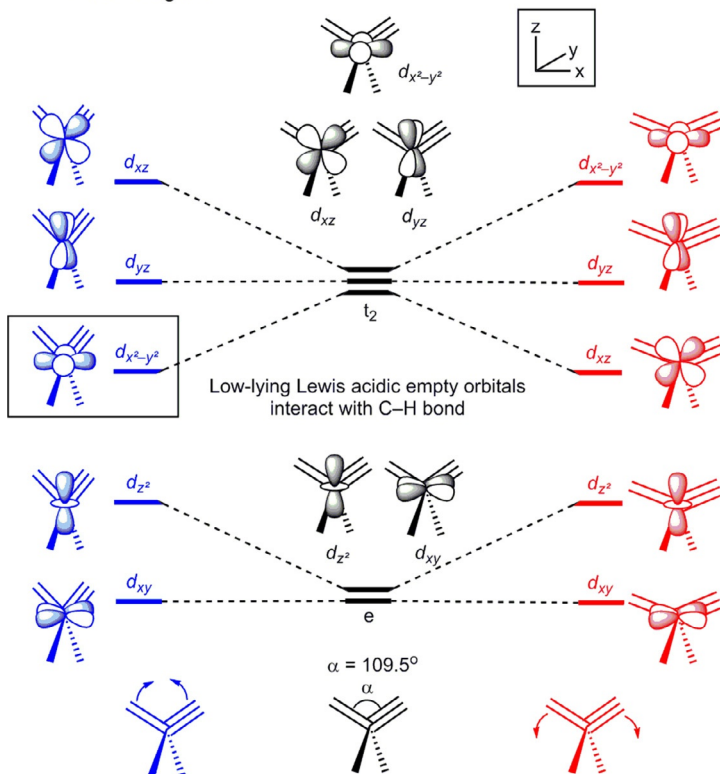Eisenstein conducted a number of theoretical studies for understanding structural and dynamic properties of Re(CR)(CHR)(X)(Y) (R = alkyl, X = Y = alkyl; X = alkyl, Y = siloxy; X = Y = alkoxy).[75] Specifically, they focused on delineating the relationship between the two possible *syn* and *anti* stereoisomers, outlined in Fig. 4A, where the presence of an α-agostic interaction between the C—H and the metal stabilizes the *syn* isomer, as previously suggested by characteristic changes in the $\nu_{C–H}$ stretching frequencies, $J_{C–H}$ NMR coupling constants, and geometrical features, which could all be reproduced reliably. The carbene rotation and hydrogen exchange processes were evaluated computationally, and it was revealed that the *syn* isomer was preferred with ancillary ligands that are pure σ-donors, whereas the *anti* isomer becomes increasingly preferred with π-donor ligands. The α-agostic interaction was found to play a key role in high-valent metal carbenes offering an effective mechanism of stabilizing the strongly Lewis acidic metal site, while activating the lengthening of the C—H bond. Interestingly, the α-agostic interaction was only present in the *syn* isomer, and increasing the number of OR groups directly bound to the metal center reduced the strength of the agostic interaction. This observation could not be rationalized by considering an increase in negative charge at the metal center as a result of the alkoxides, thus lowering the Lewis acidity, since the alkoxides are not simply added, but were exchanged for alkyl ligands that were at the coordination site before ligand exchange. To better understand this fundamental issue, the structures and electronic interactions were studied carefully, and it was found that C1–Re–C2 angles for the *syn* and *anti* isomers were less than what is expected for ideal T_d geometry, and the proposed Walsh diagram shown in Fig. 4B was in good agreement with the computed geometries. In the *syn* isomer, the decrease of the C1–Re–C2

A   Rhenium carbene complex

anti   syn
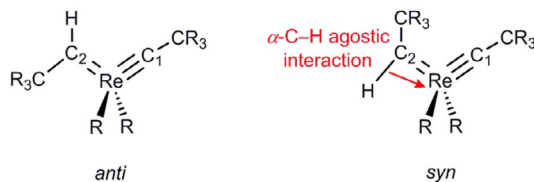
B   Walsh diagram

Fig. 4 (A) Two possible isomers for the rhenium carbene complex. (B) Walsh diagram for the metal d orbitals of a tetrahedral complex as a function of the angle between the alkylidene and alkylidyne ligands. The energy scale is qualitative.[75]

angle stabilized the $5d_{x^2-y^2}$ orbital because the out–of–phase interaction between Re and the two ligands decreases making accessible empty orbitals that can engage in Lewis acidic interactions, and promoting the α-C–H agostic interaction. In the *anti* isomer, the C—H bond no longer is correctly oriented to find an accessible empty metal d orbital.

1.2 Late transition metal alkylidenes

Transition metals in d^8-configuration are well known to form carbene complexes and they have been successfully isolated and characterized for decades. Most notably, Green characterized the first iron carbene complexes in 1967[76] and developed robust and useful synthetic methods for ruthenium and osmium carbene derivatives.[77] Iron N-heterocyclic carbenes were widely investigated and characterized, and several reports show their catalytic applications[78] in C—C bond formation[79,80], polymerization[81] and reduction.[82] From the extensive efforts made in olefin metathesis catalysis, ruthenium carbenes have become one of the representative and most thoroughly studied carbene complexes today. The development of Grubbs catalyst is described below in greater detail. Osmium carbenes are also utilized in olefin metathesis and polymerizations, just like the ruthenium carbenes.[83]

Cobalt carbenes were mostly used for cyclization to prepare aromatic compounds and furans with moderate reactivity and selectivity[84,85], and most recently found utility as catalysts for homocoupling[86] and C—H activation.[87] Generally, cobalt carbenes are formed as intermediates during catalytic cycles with several carbenoid reagents such as diazo compounds.

Dirhodium carbene and nitrene intermediates that possess three-center/four-electron bonds were shown to be special and exhibit *superelectrophilic* character. Dirhodium tetraacetate and its derivatives have been widely used to catalyze a host of important chemical transformations, involving the transfer of a carbene or a nitrene moiety to organic substrates as illustrated in Fig. 5A.[89–92] Unfortunately, little is known about their chemical and physical properties in general, since they are too unstable to be isolated, but their *superelectrophilicity* is readily recognized from the chemical reactions that they catalyze. In the absence of experimental data, a number of computational studies have been conducted to gain some fundamental insights into the catalytic reactivity.[88,93,94] Very early studies on the electronic structure of rhodium carbene complexes were based on the convention put forth by Cotton for metal-metal multiple bonding[95], and Fig. 5B describes the frontier orbital interactions between the dirhodium core and the carbene fragment. The HOMO of the carbene fragment is the σ-donor sp^2 hybrid orbital on the carbene, which donates into the Rh—Rh σ^* LUMO, whereas the empty p-orbital of the carbene fragment accepts electron density from one of the occupied high-energy Rh—Rh π^* orbitals to constitute the π-backbonding interaction. This bonding scheme is in good agreement with the general bonding paradigm established for Fischer type transition metal
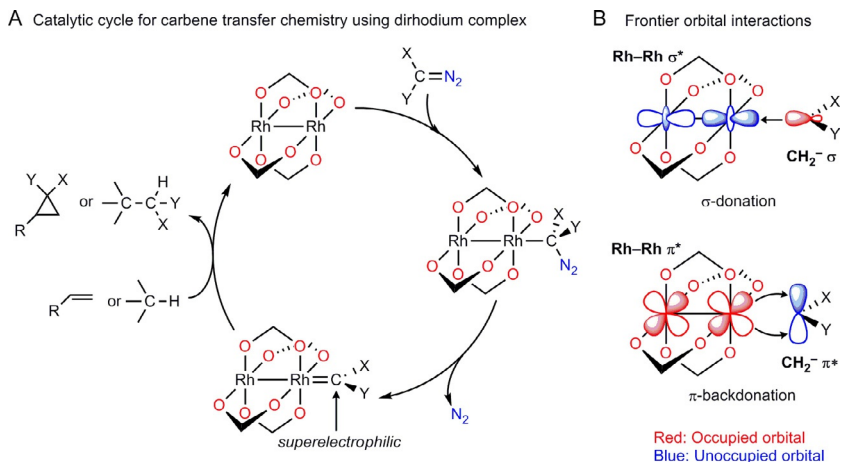
Fig. 5 (A) Catalytic cycle for carbene transfer chemistry using dirhodium complex.[88] (B) Frontier orbital interactions between the dirhodium complex core and the carbene fragment.

carbene complexes as discussed above. Whereas the exact reason for the *superelectrophilicity* is not fully understood, the formal disproportionation of the Rh(II)–Rh(II) fragment to formally afford a Rh(I)–Rh(III) moiety is thought to play an important role.

Terminal carbenes of d^{10}-transition metals are rare and are limited to *cis*-PdCl$_2${cycloC(CNMe$_2$)$_2$}(P-*n*-Bu$_3$)[101], (R$_3$P)$_2$Pd=CC$_{12}$H$_8$[102], (CO)$_3$Ni {cycloCN(R)CH$_2$CH$_2$NR}[103] and Ni{cycloCN(Mes)CH=CHNMes}$_2$.[104] These palladium or nickel alkylidenes have been typically implicated as key intermediates during Pd- or Ni-catalyzed reactions in carbene insertion processes. One representative reaction is the Pd-catalyzed cross-coupling reactions using diazo compounds as an additive that leads to a migratory insertion step after forming a Pd-carbene intermediate during the reaction as described in Fig. 6 (2).[105–107]

In addition, Hillhouse extensively studied the reactivities of Ni-carbene complexes. A three-coordinate nickel-carbene, (dtbpe)Ni=CPh$_2$ (dtbpe = 1,2-bis(di-*tert*-butylphosphino)-ethane; cod = 1,5-cyclooctadiene), was synthesized, characterized, and tested for a variety of different possible reactions.[108] Unusual group transfer reactions of Ni-carbene were achieved with nitrous oxide (N$_2$O) and organoazides (N$_3$R) to form new C=N, C=O and N=N bonds[109], or ethylene to form cyclopropane.[110] More recently, exploration of accessibility to noninteger Ni—C bond order in
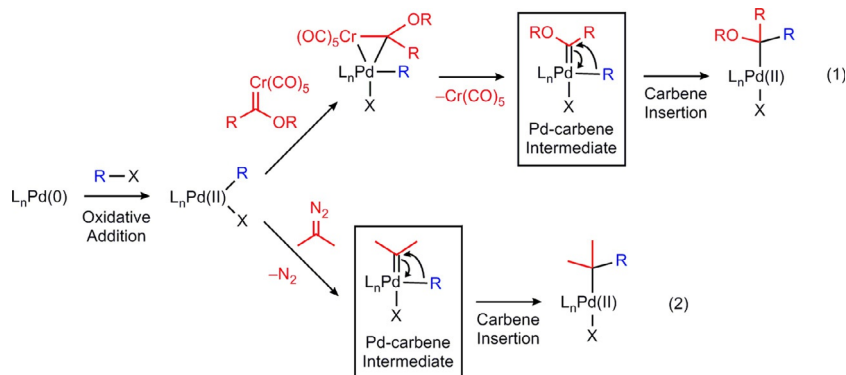
Fig. 6 Transition-metal-catalyzed cross-couplings *via* carbene migratory insertion (L, neutral innocent ligands; X, halide; R, aryl or alkyl groups).

the $(dtbpe)Ni=CPh_2$ manifold was conducted. The oxidation of $(dtbpe)$ $Ni=CH(dmp)$ $(dmp = 2,6$-dimesitylphenyl) led to internal rearrangement to form a Ni(I) system, whereas the oxidation of $(dippn)Ni=CH(dmp)$ allowed the formation of the Ni(III) carbene complex that has similar electronic configuration compared to the cationic Ni(III) imide system.[111]

Bourissou isolated a π-backdonation enhanced Au(I)–alkylidene[96] using a newly designed bisphosphine ligand tethered on a carborane cage that was attached it to a gold(I) metal center to increase the π-backbonding ability (Scheme 6). With a gold bistriflide precursor, a reaction with a diazo reagent gives a Au(I)–alkylidene complex. DFT calculations suggested that this complex is a Fischer type carbene, as highlighted in Fig. 7. Both HOMO and NLMO plot show clear π-backbonding from the gold metal center to a vacant *p*-orbital of an NHC ligand. Widenhoefer prepared a gold carbenoid complex that does not contain a heteroatom for π-conjugation.[97] Instead, the metal-carbene bond was stabilized by attaching a cycloheptatriene group. After hydride detachment, the aromatized cycloheptatrienyl cation is produced, which can be stabilized by a π-backbonding. In 2015, the analogous gold vinylidene complexes were reported by hydride abstraction followed by cyclization.[98]

Interestingly, there are some examples of gold carbene complexes showing electronic demands that are reminiscent of Schrock carbenes, namely, the carbene moiety of the metal complex shows a nucleophilic demand. Intrigued by previous work that highlighted strategies for controlling the electronic demands, Meailles first synthesized a nucleophilic Au(III)–carbene complex.[100] A geminal dianion stabilized by electron-withdrawing

A   Synthesis of Fischer-like Au(I)-alkylidene
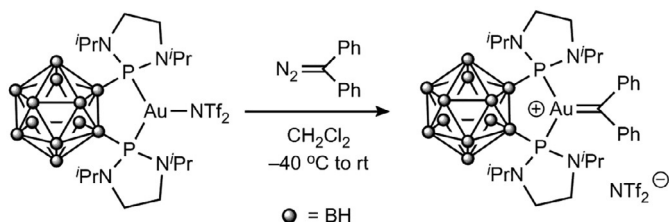
● = BH

B   Synthesis of Fischer-like Au(I)-alkylidene or vinylidene without π-conjugated heteroatoms

C   Synthesis of Schrock-like Au(I)-alkylidene
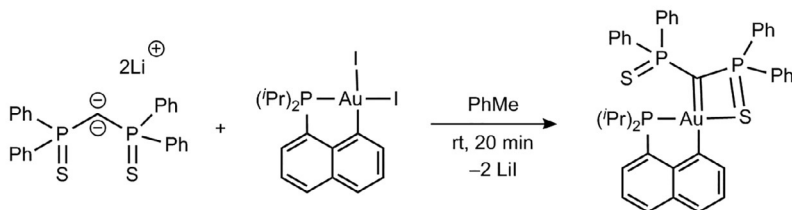
Scheme 6 Synthesis of Au(I)-alkylidene or vinylidene. (A) Synthesis of Fischer-like Au(I) alkylidene. (B) Synthesis of Fischer-like Au(I)-alkylidene or vinylidene without p-conjugated heteroatoms. (C) Synthesis of Schrock-like Au(III)-alkylidene.[96–100]
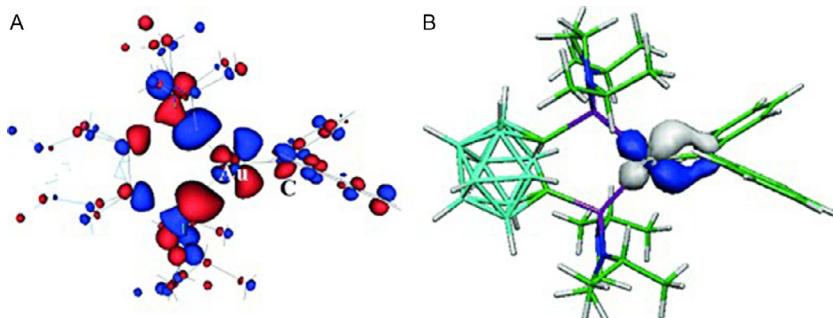
Fig. 7 (A) HOMO and (B) NLMO plot accounting for the π-backbonding from the gold metal center to a vacant p-orbital of an NHC ligand. *Adapted from M. Joost, L. Estévez, S. Mallet-Ladeira, K. Miqueu, A. Amgoune, D. Bourissou, Angew. Chem., Int. Ed. 53 (2014) 14512–14516. Copyright 2014, John Wiley and Sons.*
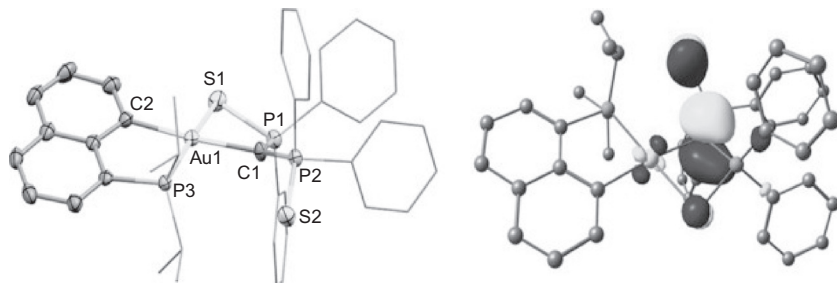
Fig. 8 Single-crystal X-ray structure (left) and representation of its HOMO as calculated by DFT (right).[100] *Adapted from A. Pujol, M. Lafage, F. Rekhroukh, N. Saffon-Merceron, A. Amgoune, D. Bourissou, N. Nebra, M. Fustier-Boutignon, N. Mézailles, Angew. Chem., Int. Ed. 56 (2017) 12264–12267. Copyright 2017, John Wiley and Sons.*

P(V) substituents were employed in combination with a Au(III) precursor and subsequent ligand exchange enabled the synthesis of a Schrock type carbene of a Au(III) complex. DFT calculations supported the nucleophilic nature of the Au(III)–carbenoid, as the HOMO of the complex shows a large orbital coefficient on the carbene carbon atom (Fig. 8), thus challenging the traditional paradigm that Schrock type carbenes require early, high-valent metals.
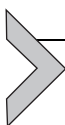
2. Computational studies on Schrock carbene: Olefin metathesis and C–X activation

2.1 Representative reactions in olefin metathesis

The metal–carbene complexes have found utility as versatile catalysts that can facilitate the transfer of various CR_2 (R: H, alkyl, aryl, amino, alkoxy) groups in olefin metathesis and other reactions. The well known examples are ring–opening metathesis polymerization (ROMP), ring–closing metathesis (RCM), cross metathesis (CM), and acyclic diene metathesis (ADMET), as shown in Fig. 10A.[1,114,115] The reaction mechanism that was initially proposed, Chauvin introduced the idea that the metal–carbene can engage the olefin substrate *via* a [2 + 2] cycloaddition resulting in a four-membered metallacyclobutane intermediate[8,116], as outlined in Fig. 9. The olefin metathesis leading to a novel olefin is accomplished by a reverse cycloaddition. On first sight, this proposal is difficult to accept, as the analogous [2 + 2] cycloaddition with standard organic olefins is symmetry-forbidden according to the Woodward-Hoffmann rules and requires photochemical conditions.[117] Over the years, support for this mechanism grew and it
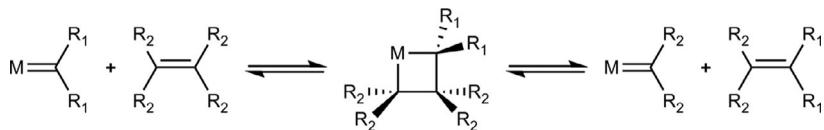
Fig. 9 Mechanism for olefin metathesis proposed by Chauvin.

was recognized that the role of the metal-center is to distort the shape of the π-orbital to an extent that the $[2+2]$ cycloaddition becomes non-synchronous and by forming the C—C and M—C bonds in a stepwise manner, the orbital-symmetry forbidden reaction can be accomplished. Chauvin's mechanism is now generally accepted and the four-membered metallacyclobutane intermediate has been thoroughly investigated both experimentally[118–128] and computationally.[129–139] The insights derived from these studies proved valuable for improving the performance and utility of the catalyst. One of the earliest computational studies employed extended Hückel calculations to identify the electronic features of the intermediate metallacycle.[140]

Although the initial studies were motivated by olefin metathesis as a means for preparing polymers and extending the carbon chain length by starting with two medium sized olefins to access one olefin with a much longer carbon chain and another with a much shorter carbon chain as a side product, olefin metathesis has gained tremendous popularity as a generic method for selective C—C bond formation. Especially, the catalysts pioneered by Grubbs have become indispensable tools in synthesis including the preparation of natural products. Two representative cases of a total synthesis of complex natural product, where olefin metathesis played a key role, are shown in Fig. 10B. Specifically, the (Z)-selective ring–closing metathesis is the key step required for the efficient synthesis of nakadomarin A. In a different example, a metal-carbene catalyst was employed[112] to facilitate a cross metathesis step that combined two olefin components together to successfully prepare neopeltolide, an anti-tumor agent.[113]

Most widely used among the olefin metathesis catalysts are Grubbs first and second generation catalysts. First described in 1992, this first example of an alkylidene complex of ruthenium used triphenylphosphine as an ancillary ligand.[83] In addition to much experimental work, these systems have also inspired many computational studies. It was revealed that a main challenge in the first generation Grubbs catalyst lies in the fact that the threefold symmetric phosphine ligand must be rotated for the catalyst to become active, which caused a notably higher barrier than for the second generation
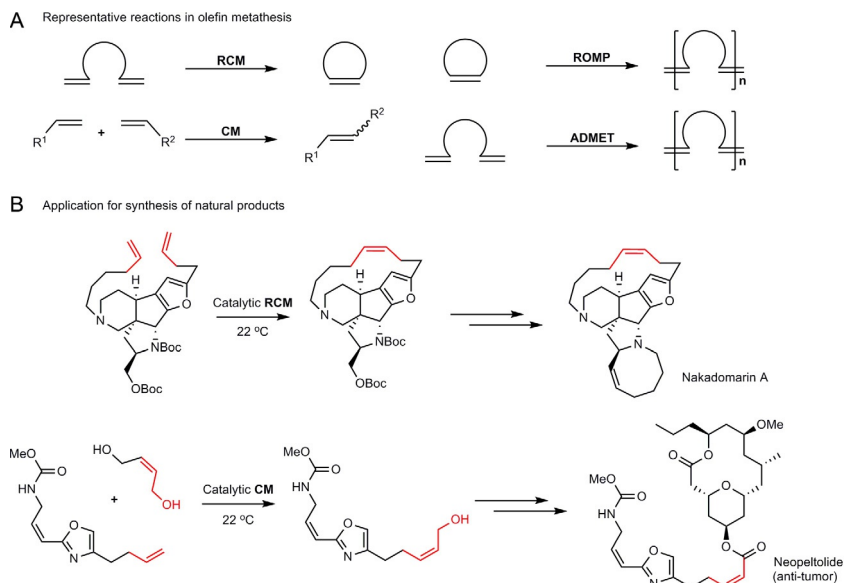
Fig. 10 (A) Representative reaction in olefin metathesis (RCM, ring-closing metathesis; CM, cross metathesis; ROMP, ring-opening metathesis polymerization; ADMET, acyclic diene metathesis). (B) Recent application of olefin metathesis reactions to synthesis of natural products such as nakadomarin A and neopeltolide.[112,113]

catalyst, where the NHC ligand shows a twofold symmetry and the necessary rotation barrier is absent.[136]

Even though directly joining two olefins with M=C double bond has been recognized as an important and ubiquitous strategy in organic synthesis, several issues needed to be solved in order for olefin metathesis to become an universally useful methodology. First, catalyst stability was a major concern, as the early catalyst systems easily decomposed during the reaction, whereas the reactivity needed to be increased to give fast and clean reactions. Lastly, the first generation lacked stereoselectivity affording synthetically less useful mixtures of products. Developing catalytic olefin metathesis reactions that are (Z)-selective is particularly difficult because (Z)-alkenes are often energetically disfavored over their (E)-analogs. The emergence of olefin metathesis as a standard method in the tool of synthetic organic chemists is in part the result of some remarkable progress that was achieved in the past in developing new catalysts that showed high levels of stability, reactivity and selectivity[141], including the aforementioned E/Z-selectivity.[142] Computational studies played an important role in overcoming the initial problems[143] and contributed to both understanding experimentally observed properties and establishing principles of catalyst design for performance improvement.

2.2 Olefin metathesis using Schrock type catalysts

Following the paradigm of early transition metals in high oxidation states, many Schrock type metal alkylidene or alkylidyne complexes have been prepared and tested as olefin metathesis catalysts, some notable examples of which are represented in Fig. 11. Earlier work focused on molybdenum and tungsten, and alkoxy ligands were particularly successful in stabilizing the catalyst, while enhancing the reactivity at the same time. In addition, isopropyl (^{i}Pr) or tertiary butyl (^{t}Bu) functional groups were used for creating a sterically hindered environment to prevent decomposition of catalysts through interaction between two reactive alkylidene complexes and dimerizations that involve metal–metal bond formations. Early catalysts, such as **30** or **32**, were modified with different alkoxy or imido ligand to give new systems, such as **31** and **33**. Chiral bidentate O-based ligands were also used to prepare catalysts like **34** and **35** that found utility in asymmetric synthesis. And recently, unsymmetrical catalysts (**36**, **37**) with two different monodentate ligands have been used for increasing the reactivity. In Fig. 11 only one stream of representative development is given to offer a historical perspective, and similar developments can be seen in tungsten and rhenium catalysts.[75,151,152]

Although a rough conceptual sketch of the mechanism was provided by Chauvin, many details remained unclear and many experimental studies faced limitations that did not allow for providing all the details needed to construct a precise and atomistically detailed mechanism. Computational studies have made significant contributions[143], and several mechanistic features were
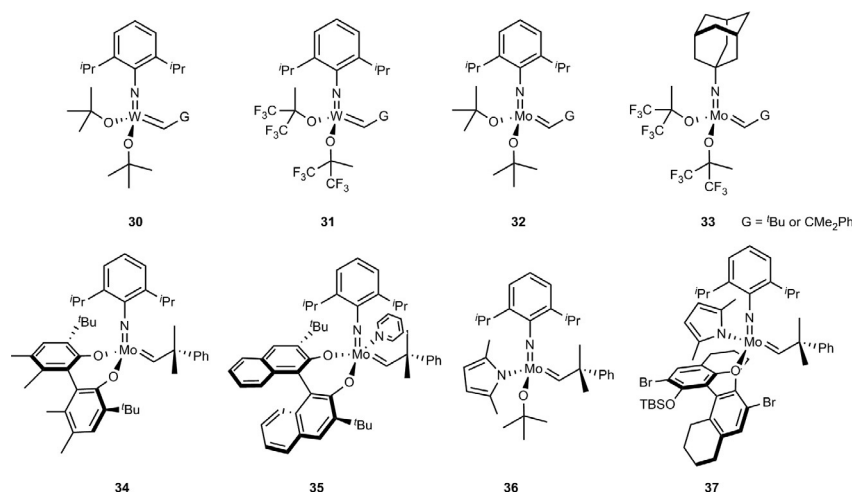
Fig. 11 Schrock catalyst at the early stage of development (**30 – 33**) and Schrock catalyst improved through various theoretical rationalization (**34–37**).[144–150]
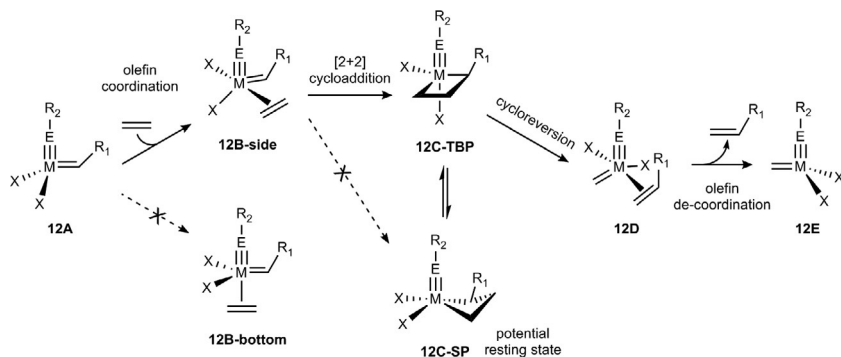
Fig. 12 Generally accepted mechanism for olefin metathesis reaction (M = Mo and W; E = N; M = Re, E = C).

revealed as illustrated in Fig. 12: (i) The C—C σ-bonds forms after the olefin first engages the metal to first form an olefin-adduct. (ii) Olefin binds at the *trans* position of X (side attack, **12B–side**) rather than at the *trans* position of E (bottom attack, **12B–bottom**) in **12A** → **12B** step. This detail was revealed later to be important for controlling the selectivities of this class of catalysts. (iii) The coordination of olefin is accompanied by a structural distortion from tetrahedral to trigonal bipyramidal. (iv) There are two possible isomers in the four-membered metallacyclobutane intermediate having trigonal bipyramidal (**12C–TBP**) and square pyramidal (**12C–SP**) geometry. (v) There maybe no direct pathway traversing from **12B** to **12C–SP**.

Computational studies on molybdenum carbenes and their catalytic activity in olefin metathesis were carried out by Ziegler in the 1990s.[129] Initial focus concerned the structure of the metallacyclobutane, where two possible intermediate geometries, the trigonal bipyramidal and square pyramidal coordination structures were considered in a model system $L_2Mo(X)CH_2$ (L = Cl, OCH_3 and OCF_3; X = O and NH). Inspecting the frontier orbitals of the free carbene, square pyramidal and trigonal bipyramidal framework, it was suggested that the decomposition of the square-pyramidal intermediate occurred without traversing a trigonal-pyramidal structure. The alkene addition through a side-on attack was examined in detail by Peng using severely simplified models, namely, $Mo(NH)(CHR)(OR')_2$ (R = H, Me; R' = CH_3, CF_3).[131] There is a significant preference for ethene to attack the CNO face over the COO face of the catalyst, which was computed to be 12.3 and 18.8 kcal/mol for R' = CH_3 and CF_3, respectively. Structural change to distorted trigonal bipyramidal geometry has been calculated to be an important feature when ethene attacks at the CNO face. The

disadvantage of bottom attack can be also rationalized with a rotation of the $[CH_2]^{2-}$ ligand, which energetically is somewhat demanding but is necessary to form the metallacyclobutane intermediate due to the initially mismatched symmetry of π-orbitals. In addition, the molybdacyclobutane significantly favors a square pyramidal geometry when R'=CH_3, but has a slight preference for a trigonal bipyramidal geometry when R'=CF_3. This study offered some clue that the catalytic activity could be enhanced if electron-withdrawing O-based ligands were employed for the Schrock type catalyst (**31**, **33**) to prevent decomposition of catalyst through remaining as square pyramidal metallacyclobutane intermediate.

Studies aimed at constructing a full reaction pathway using $[(MeO)_2Mo(CH_2)NH]$ as a model system were conducted[153] and one of the main questions was whether $[2+2]$ cycloaddition takes place in an one-step process or requires several steps that include initial coordination of the metal and olefin that can then move on to form the metallacyclobutane in a two-step process. Calculations showed that structural distortion of the molybdenum carbene from tetrahedral to square pyramidal geometry is required to accommodate the side-on coordination of incoming ethylene, which is associated with a small barrier for the near isothermic generation of the ethylene adduct. The C—C σ-bonds are still far from their equilibrium distance in the transition state of $[2+2]$ cycloaddition. These results indicate that ethylene adduct formation before cyclization is likely pointing to a two-step reaction mechanism.

Based on the general mechanism of the olefin metathesis that emerged from many experimental and computational studies, many researchers devised strategies for improving catalytic processes. Among the issues in olefin metathesis, stereoselectivity has been of particular interest. Early studies indicated that stereoselectivity could be engineered into catalysts by employing various bulky and chiral ligands[114], and one of the early applications was reported by Crowe and Zhang in 1993.[154] Enantioselective olefin metathesis reaction was also achieved with Mo complexes such as **37**[155] that were stereogenic at the metal center. As illustrated in Scheme 7, an enantioselective olefin metathesis reaction was successfully achieved employing catalyst **34** with biphenolate ligand by Schrock.[156] The full mechanism of the intramolecular asymmetric ring-closing metathesis was constructed and studied with DFT calculations.[153]

One of the remarkable advantages of the Schrock type catalysts over the Fischer type systems is that they are typically much more reactive and need mild conditions to accomplish olefin metathesis. Eisenstein has studied this
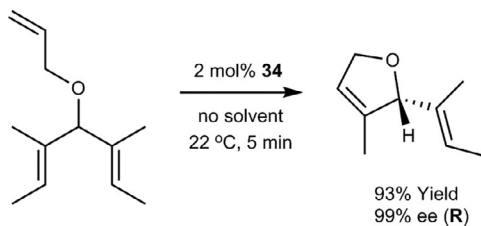
Scheme 7 Asymmetric ring-closing metathesis (ARCM) using **34**.[156]

general observation in a series of studies. Even though the majority of the research in olefin metathesis has focused on the symmetrical Schrock catalysts, $[M(\equiv ER)(=CHR)L_2]$ (M=Mo and W; E=N; M=Re, E=C), meaningful predictions could be made for the unsymmetrical Schrock catalysts such as, $[M(\equiv ER)(=CHR)(X)(Y)]$ as well, that were thought to have much potential to be better catalysts.[75,152,157] The full reaction mechanism of olefin metathesis catalysis was described using both symmetrical and unsymmetrical catalysts to compare their catalytic efficiencies in an effort to identify characteristic differences, as illustrated in Fig. 13, utilizing alkyl, alkoxy, and siloxy ligands to create the appropriate ligand sets. There were two key factors that were found to determine the shape of the potential energy surfaces: (i) the distortion energy of the initial tetrahedral catalyst to form the olefin–adduct intermediate and (ii) the stability of the metallacycle intermediate. In terms of olefin coordination step (**13A–TS**), the structural distortion energy of the catalyst was the most important and determined the activation barrier, because the olefin and the metal were still far from each other (>3 Å) at the transition state to give only a small structural distortion energy upon binding ethene and an equally small metal–olefin interaction energy. The low barrier of **13A–TS** of the unsymmetrical catalyst shown in blue is only 0.8 kcal/mol, but other symmetrical catalysts marked in black and green have ~5 kcal/mol higher activation barrier.

These energies were rationalized using a qualitative MO diagram for the olefin addition, shown in Fig. 14. In the transition state of the olefin coordination, the metal fragment has a trigonal pyramid geometry and the $d_{x^2-y^2}$ orbital is destabilized by σ-donor orbitals of the Y ligands. These interactions increase the energy gap between the empty $d_{x^2-y^2}$ orbital and occupied p orbital of the triply bonded E ligand. Thus, a decrease in $d_\pi-p_\pi$ interaction strength weakens the M$\equiv$E π interaction and the electron density of the M$\equiv$E bond is polarized toward E ligand at the transition state. On the other hand, the structural distortion energy is decreased when the strong σ-donor found the most available metal orbital to maximize its bonding interaction,
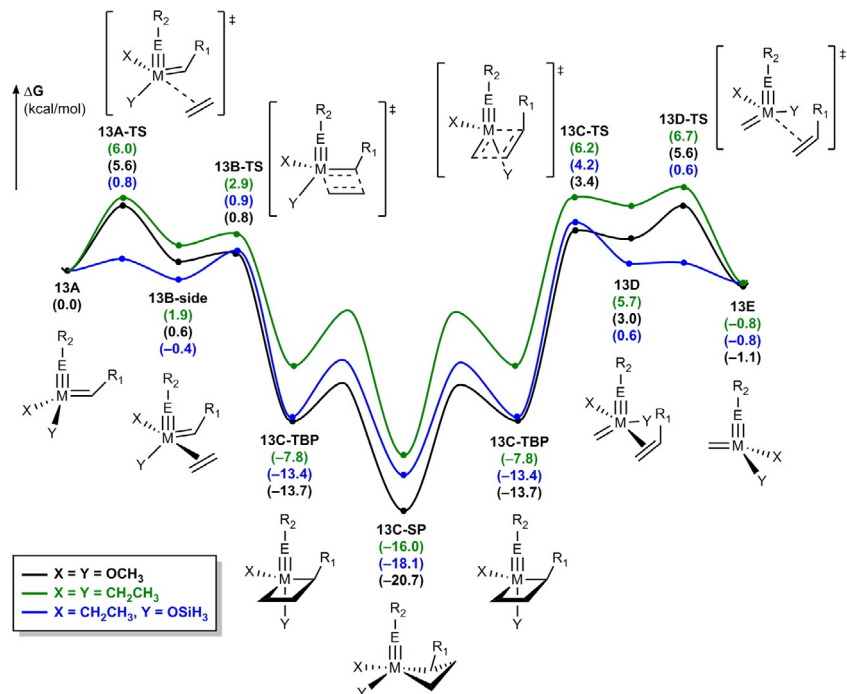
Fig. 13 Reaction energy profile for the olefin metathesis of C_2H_4 with $Mo(N\equiv CH_3)$ $(=CHCH_3)(X)(Y)$ as a model system.
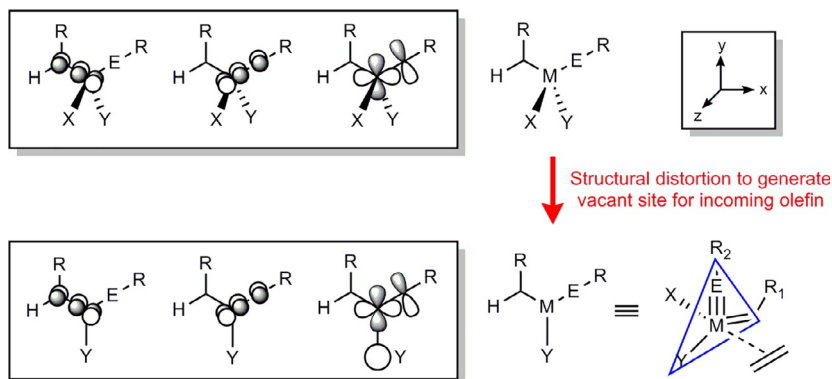
Fig. 14 Qualitative molecular orbital diagram in coordination of olefin step.

thus, it is located in the *trans* disposition to the vacant site.[152] Combining these two effects, it was concluded that one poor σ-donor and one good σ-donor are better for catalyst activity as the olefin–adduct intermediate formation becomes favorable.

Another important factor that determines the shape of a potential energy surface is the relative stability of **13C–SP** shown in Fig. 13. As mentioned above, deactivation of catalyst through the square pyramidal metallacyclobutane has been implicated repeatedly[158–161], and a shallow potential energy surface was deemed a desirable feature that may prevent decomposition of catalyst and production of side products. The stability of the metallacyclobutane intermediate is controlled by the M–C bond strength, which increases with the number of O-based ligands. Combining these two conclusions, a good compromise was reached by synthesizing unsymmetrical catalysts that have different X (good σ-donor) and Y (poor σ-donor) ligands. This general insight derived from calculations was slowly embraced by the experimental community. The early olefin metathesis reactions employed symmetric catalysts with two O-based ligands, but gradually began using asymmetric catalysts, such as monoalkoxide pyrrolide (MAP) complexes (**36**, **37**), which increased the catalytic efficiency notably[149,162], boron-containing complexes[163], and the silica supported systems[164,165] have also been tested and continue to inspire much work.

2.3 C—H activation using Schrock type metal alkylidene

M=C bonds were found to be useful motifs for facilitating a variety of other reactions, e.g., C—H activation *via* 1,2-addition.[166] Although metal carbene complexes generally undergo heterolytic C—H bond cleavage due to the high degree of polarization typically found in M=C bonds, late metal carbenes often form electron-rich metal centers capable of oxidatively deprotonating C—H bonds to give metal hydrides[167], whereas early metal carbenes can increase the nucleophilicity of the carbene to a point that deprotonation of other hydrocarbons becomes feasible. These two reactivity patterns either on the metal or on the carbene sites have served as a fundamental principle, upon which much of the reactive chemistry of metal alkylidenes could be developed. The intermolecular C—H activation of hydrocarbon substrates, benzene and *p*-xylene by titanocene alkylidene intermediates[168] was observed relatively early and has been known for a long time. These thermal activations of C—H bonds were achieved by transiently generated Cp*W(NO)(=CHCMe$_3$) complexes that were prepared *in situ* from Cp*W(NO)(CH$_2$CMe$_3$)$_2$. Experimentally identifying and studying these reactive intermediates proved difficult and some success was reported by using excess amounts of PMe$_3$ to stabilized a neopentylidene intermediate to form Cp*(NO)W(=CHCMe$_3$)(PMe$_3$).[169] Computational studies on the activation of substituted arene complexes such as toluene, showed that the C

(sp^3)—H of the methyl group is much more difficult to activate than the C (sp^2)—H bond of arene.[170,171] Similarly, benzene and pyridine activation reactions by a vanadium(III) alkylidene were extensively studied by Mindiola and Baik.[172] Taken together, these studies have shown that early transition metal alkylidenes constitute a remarkably reactive class of molecules that are capable of carrying out a number of challenging chemical reactions.

3. Titanium alkylidyne: Super Schrock carbyne generated from Schrock carbene

An intriguing avenue that was considered even in the early stages of the exploration of metal carbene chemistry is to employ the metal carbynes to carry out various reactions, and some notable successes were reported throughout the last few decades.[1] At the time the Fischer carbenes were discovered, only a few examples of metal carbynes were known, but a number of new complexes containing metal-carbon triple bonds with chromium, molybdenum, and tungsten centers were discovered in 1973.[173] Analogous to the metal carbene complexes, the metal carbynes can also be divided into two classes, the Schrock type and Fischer type carbynes. To date, there are only a handful known examples of Fischer type carbynes[174], and most known examples belong to the Schrock type carbynes.[175–179] Various transition metals having a metal-carbon triple bond were synthesized and fully characterized[40,47,174,180–182], and used as a catalyst for olefin metathesis and other interesting reactions.[183–191] Scheme 8 shows one specific example of how a metal alkylidyne complex can be prepared.[40,47]
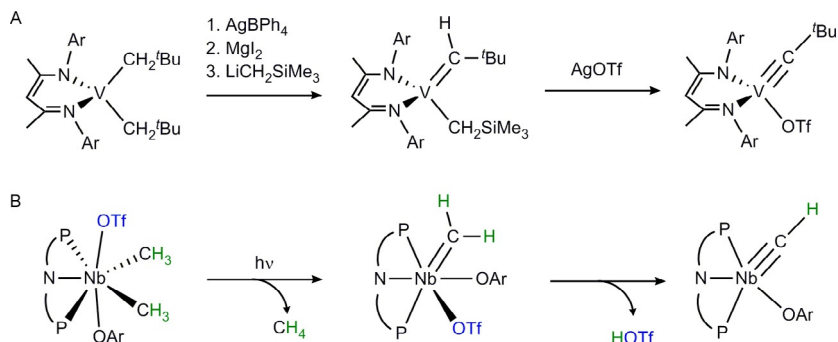
Scheme 8 Synthesis of early metal alkylidyne complex. (A) Vanadium alkylidyne complex. (B) Niobium alkylidyne complex.

Considering the conceptual understanding of the electronic structure of the Schrock carbenes, the prospect of accessing titanium–carbon triple bonds is exciting. The carbon center on Schrock carbene is already considered highly nucleophilic and formally negatively charged. As was discussed above, much of the special characteristics and chemical reactivities are based on the nucleophilicity of the carbon. In principle, the Schrock carbyne can be imagined to be the product of deprotonating a Schrock carbene. Thus, one may speculate that the nucleophilicity of the Schrock carbyne is much more enhanced when compared to the analogous carbene. Therefore, initial attempts to access this new class of molecules focused on deprotonating, for example, titanium alkylidenes as shown in Fig. 15A using a strong Brønsted base, such as *tert*-butoxide. Naturally, many of these alkylidynes are expected to be highly reactive and difficult to isolate and study—thus, computational methods became a particularly useful and indispensable tool for studying and understanding these reactive molecules. Generally, alkylidyne complexes are often derived from alkylidene complexes by α-hydrogen abstraction reactions. Mindiola and Baik reported the first study that strongly suggested that titanium alkylidynes exist as transient, reactive intermediates using both experimental and computational methods in 2005[192] and 2007.[193] The parent carbene complex, a relatively stable low-coordinate titanium alkylidene compound with a nacnac ligand (nacnac = [Ar]NC(Me)CHC (Me)N[Ar]$^-$, Ar = 2,6-(CHMe$_2$)$_2$C$_6$H$_3$), was often fraught with undesirable side reactions because of the inherent reactivity of the imine functionality. To avoid these stability obstacles, PNP pincer type ligand (PNP = N-[2-P(CHMe$_2$)$_2$-4-methylphenyl]$_2^-$) was considered as a new tridentate ligand framework that may offer higher stabilities. Computational explorations of the rigidity of the ancillary ligand frameworks clearly
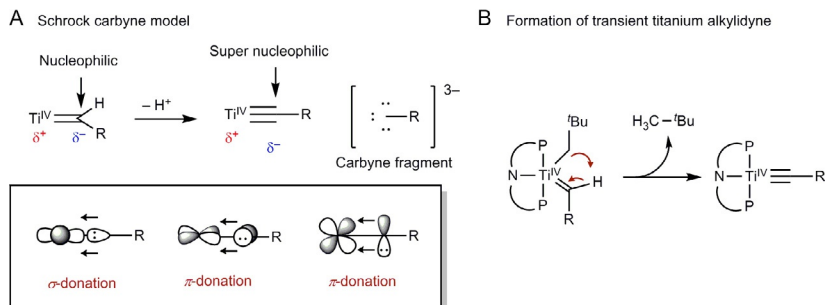

Fig. 15 (A) Bonding scheme of Schrock carbyne complex. (B) Formation of transient titanium alkylidyne through an α-hydrogen abstraction.

indicated that PNP is much more preferable over nacnac, as PNP allowed for a "hybrid type" coordination combining both of a hard amide and two soft phosphine donors, while sterically hindering the tridentate geometry from distorting its basic coordination geometry pattern. These structural characteristics made PNP much more suitable for accommodating and stabilizing the titanium alkylidene moiety while avoiding intramolecular cross metathesis type of reactions that may lead to decomposition.[194] Finding such stable ligand frameworks has been a strong driving force in subsequent studies and the Mindiola-Baik team has established a simple and well-understood foundation for accessing the titanium-carbon triple bond species, a prominent example of the Schrock-carbyne class of molecules, as illustrated in Fig. 15B. Despite significant experimental efforts, it has thus far not been possible to detect and characterize the titanium alkylidyne directly and most of the structural and chemical properties are derived from computational studies that are benchmarked and tested indirectly by matching computations against experimental results.

One key evidence for the existence of the titanium alkylidyne is offered by the calculated reaction energy profile for conversion from $(PNP)Ti=CH^tBu(CH_2^tBu)$ to $(PNP)Ti=CH^tBu(C_6H_5)$ in benzene as illustrated in Fig. 16.[193] The $(PNP)Ti=CH^tBu(CH_2^tBu)$ complex first undergoes α-hydrogen abstraction, traversing the transition state at 27.8 kcal/mol to form the hypothetical adduct intermediate **16B**. Extrusion of neopentane leads to titanium alkylidyne, and the relative free energy of 4.6 kcal/mol is only slightly higher than the starting complex, which means that the proposed titanium alkylidyne may be able to exist as a minor component of an equilibrium. This titanium alkylidyne species can activate the C—H bond of benzene to afford $(PNP)Ti=CH^tBu(C_6H_5)$. This energy profile suggests that the titanium alkylidyne intermediate may be detected directly, if the benzene activation is sufficiently slow. Initial attempts were not successful and modifications of the ligands and experimental conditions may be necessary. This goal is still being pursued in the Mindiola-Baik laboratories.

Even though the reaction energy profile shown above is reasonable, some questions can be raised about other plausible mechanistic possibilities. For example, unsaturated M=C linkages that are generated as products can undergo C—H activation without traversing the putative titanium alkylidyne intermediate. To preclude this possibility, the transition state energy of direct C—H activation after forming the six-coordinated benzene adduct of $(PNP)Ti=CH^tBu(CH_2^tBu)$ was calculated to show an
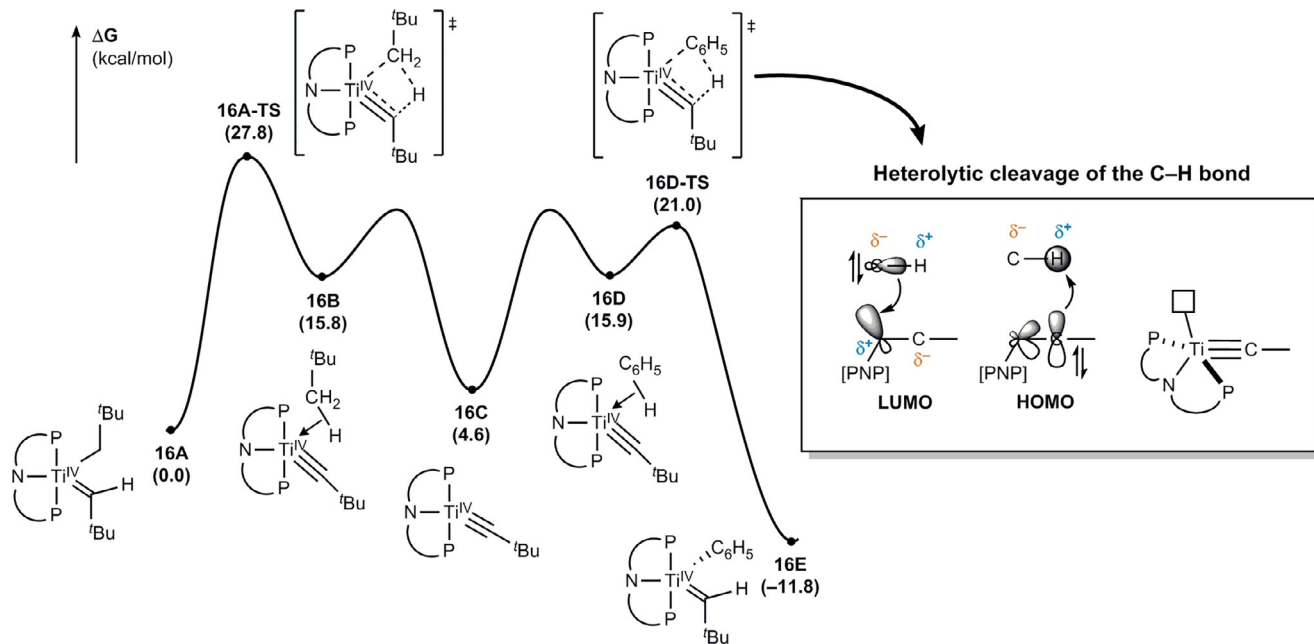
Fig. 16 Computed reaction energy profile for 16A ⟶ 16E conversion in benzene ($\varepsilon = 2.284$). Relative energies in kcal/mol are given in parentheses.[193]

unrealistically high relative free energy of 53.3 kcal/mol. In addition, disso-
ciation of one phosphine arm of the PNP ligand was considered to decrease
the steric hindrance during C—H activation, but these transformations
were also found to be associated with very high energies. The C—H
activation *via* the titanium alkylidyne was the most reasonable reaction
pathway in these studies.

There are two possible formal mechanisms by which the C—X bond
activation can take place: (i) homolytic bond cleavage *via* Ti(III)≡C• and
(ii) heterolytic fashion *via* standard Lewis acid/base binding. The charge
distribution at the titanium alkylidyne moiety during the reaction with
neopentane and benzene was obtained using calculated electrostatic poten-
tials (ESPs). At the alkylidyne carbon, a charge of −1.38 was found, whereas
+1.37 was calculated for titanium, in good agreement with the conceptual
understanding of the bonding in titanium alkylidyne complexes.

The computationally obtained geometry showed that the Ti≡C bond
length is 1.749 Å, and this distance is significantly shorter than Ti═C and
Ti—C that are typically found to be ∼1.85 and ∼2.14 Å, respectively. This
short bond length was a strong indicator of the proposed titanium–carbon
triple bond, and molecular orbitals of titanium alkylidyne structure were
also found to support this assignment, as shown in Fig. 17. The Ti—C
σ-bonding was located at HOMO-5, and HOMO and HOMO-1 indicated
two π-bonding orbitals. Furthermore, it was found that the binding of
additional ligands does not affect the electronic structure and geometry
due to the empty coordination site being dominated by the LUMO,
allowing a highly localized binding event for the additional substrate. This
feature was identified as one of the key characteristics of the titanium
alkylidyne complex enabled by the PNP ligand framework that allows for
a highly versatile reactive chemistry to be displayed.

3.1 C—X (X = H, O, F, N) activation

The discovery of the reactive titanium alkylidyne complex led to the explo-
ration of various other strong bonds that may be amenable to activation. As
illustrated in Scheme 9, C—O and C—F bond activation[195] and
ring–opening of pyridine[196,197] were also observed successfully using the
transient titanium alkylidyne. Aliphatic $C(sp^3)$—H activation of linear or
cyclic alkane was found[198,199], and finally, the extremely high reactivity
of titanium alkylidyne has been demonstrated by the fact that it can activate
the C—H bond of methane gas at room temperature.[200]

A   HOMO-5 (-6.470 eV)   B   HOMO-1 (-3.983 eV)

$d(z^2)$ $d(yz)$

C   D

$d(xz)$ $d(x^2-y^2)$

HOMO (-3.756 eV)   LUMO (-0.928 eV)
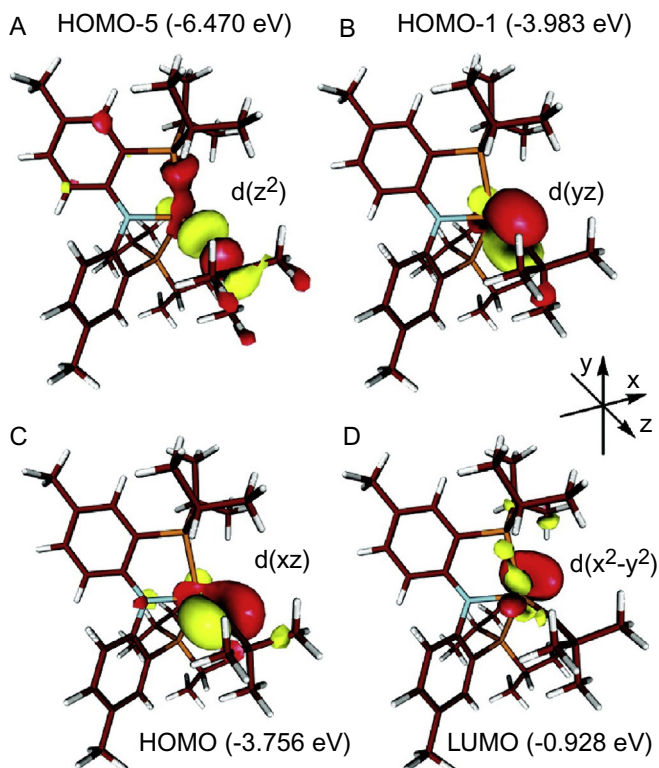
Fig. 17 Most important molecular orbitals of titanium alkylidyne (isodensity = 0.05 au). (A) Ti–C σ-bonding orbital. (B, C) Two Ti–C π-bonding orbitals. (D) LUMO of titanium alkylidyne.[193] *Adapted from B.C. Bailey, H. Fan, J.C. Huffman, M.-H. Baik, D.J. Mindiola, J. Am. Chem. Soc. 129 (2007) 8781–8793. Copyright 2007, American Chemical Society.*
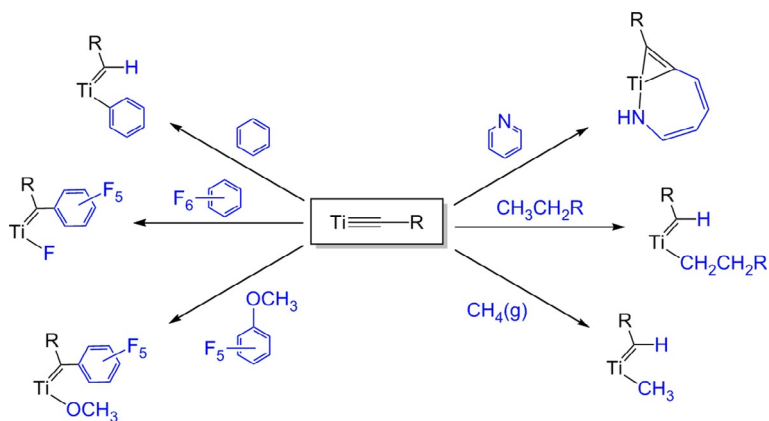
Scheme 9 Investigations of the reactivity of titanium alkylidyne. PNP ligand is truncated for clarity.

3.2 C—F and C—O activation

In an effort to trap or at least stabilize the titanium alkylidyne intermediate long enough to obtain spectroscopic evidence of its existence, various solvents, additive and reaction conditions were tried that were initially designed to prevent any reactions. For example, the alkylidyne was generated in per-fluorinated solvents, such as C_6F_6 and $CF_3C_6F_5$, with the hope that the lack of any bonds that could be attacked may allow for directly observing the alkylidyne. During this process, it was discovered that the titanium alkylidyne intermediates are capable of activating C—F and C—O bonds following a similar mechanism as seen previously with C—H bonds, namely, 1,2-addition across the M—C triple bond.[195] In contrast to benzene activation, inter-molecular activation of C—F and C—O bonds of arene showed that the α-carbon performed a nucleophilic attack on the carbon site instead of the fluoride or methoxy group due to different charge separation compared to benzene. This experimental result was also consistent with the general concept of highly polarized titanium-carbon triple bond. Electron-deficient carbon could be coupled with α-carbon of titanium alkylidyne, whereas electron-rich fluoride was coupled with titanium.

3.3 C(sp^3)–H activation

This titanium alkylidyne could also be reacted with linear or cyclic alkanes, and ultimately led to dehydrogenated olefin product at room temperature via C(sp^3)—H activation as well as C(sp^2)—H bond activation of benzene as represented in Scheme 10.[198,199] Whereas dehydrogenation of unactivated alkanes is known[201], these reactions required precious metals such as iridium and harsh conditions. Although the catalytic turnover numbers were low, this example of a titanium alkylidyne complex dehydrogenating various unactivated alkanes including cyclohexane to afford the corresponding alkenes is the first report of a base metal carrying out such a reaction under mild conditions. Mechanistically, DFT-calculations indicated that the dehy-drogenation takes place without a β-hydride elimination step, which is attrac-tive, because the migratory insertion of an olefin, which would be the microscopic reverse reaction, can be avoided. Key to closing the catalytic cycle was the use of a phosphorus ylide to regenerate the titanium methylidene which immediately gave tautomerized titanium methyl alkylidene[202], offering a solution to a long standing problem of how to turn the often stoichiometric reactions of the titanium alkylidyne reagent catalytic, where the key issue has always been about recovering the catalyst and reforming a catalytically active species.
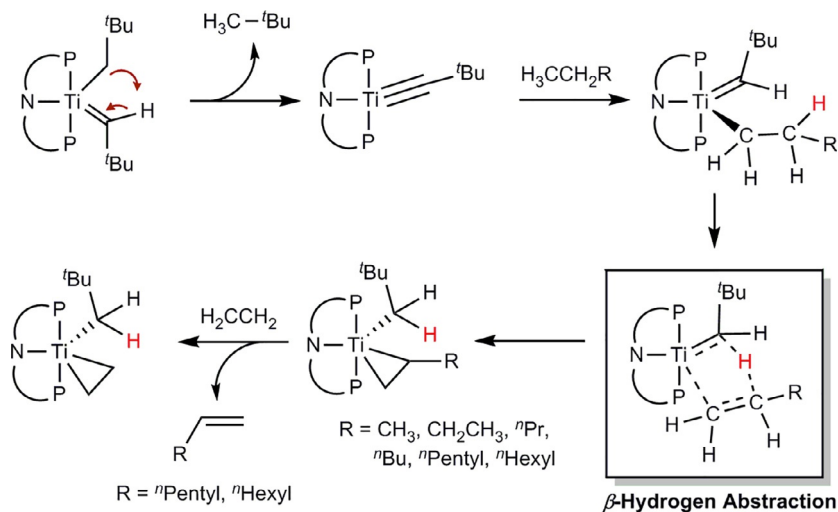
Scheme 10 Dehydrogenation of linear alkanes through a β-hydrogen abstraction.

3.4 Ring-opening of pyridine

In addition to intriguing C—X (X=H, O, F) activation, it was also discovered that the PNP stabilized titanium alkylidyne species can ring-open N-heterocycles such as pyridine or picoline. This was a remarkable discovery, since ring-opening pyridine is a difficult reaction that only a handful systems have been able to achieve[203–206], but also because the ring-opening occurred selectively without the possible C—H activation of N-heteroarenes[196] that should be easier to perform. The ring-opened products were found to undergo complete removal of nitrogen affording carbon-only products when an electrophile such as $(CH_3)_3SiCl$ was added[197], thereby completing a full denitrogenation cycle. The mechanism of the C—N bond cleavage that accompanies the pyridine ring-opening was examined in detail, as breaking such a strong bond is intriguing and there is significant interest in such processes for industrial scale hydrodenitrogenation (HDN) for the catalytic conversion of N-heterocycles present in petroleum or coal-based liquids to ammonia, which would produce nitrogen-free carbon based petroleum and coal products of substantial commercial interest.

Fig. 18 summarizes the proposed mechanism of the ring-opening reaction, which proceeds *via* nucleophilic attack of the Ti≡C moiety on the C2 of pyridine, instead of C—H bond cleavage mentioned above. After forming the transient titanium alkylidyne intermediate by extruding the neopentane, the Lewis basic pyridine coordinates to the vacant site of
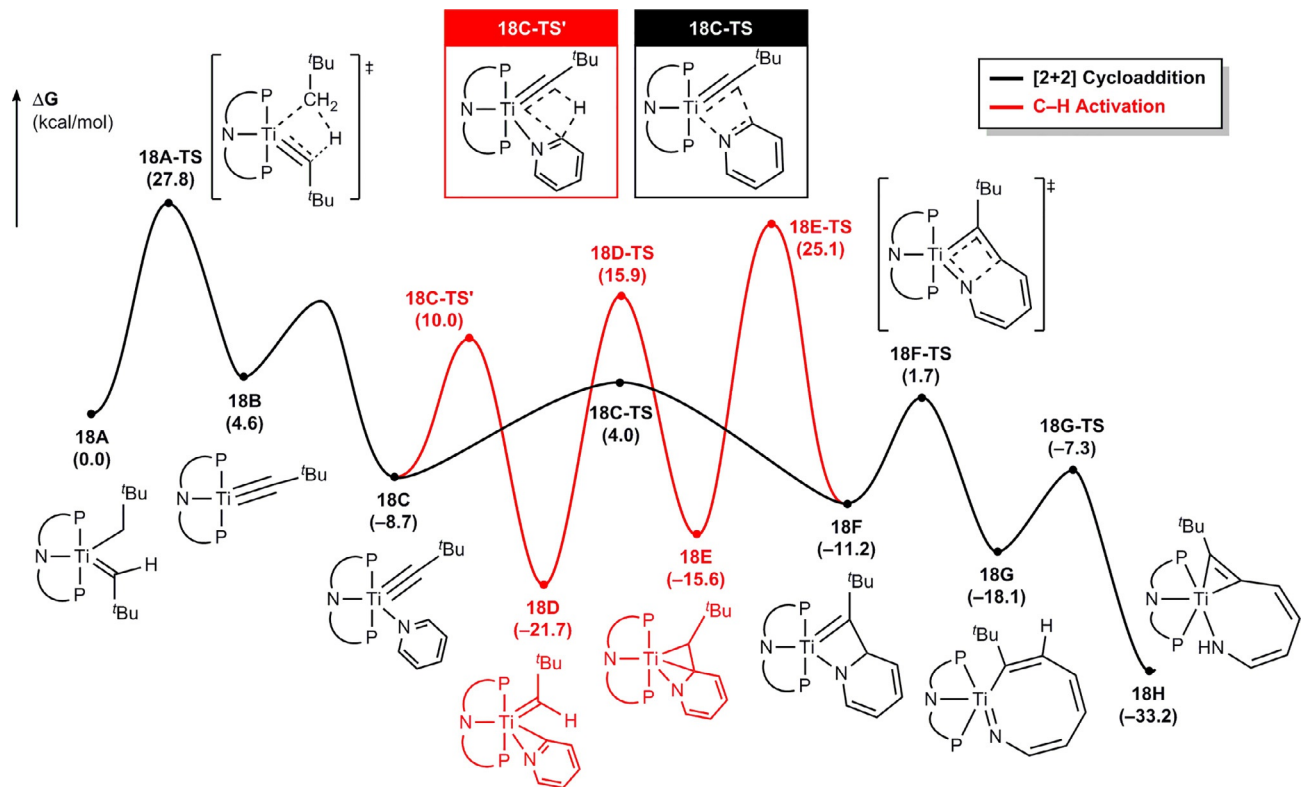
Fig. 18 Proposed mechanism for pyridine ring-opening reaction.
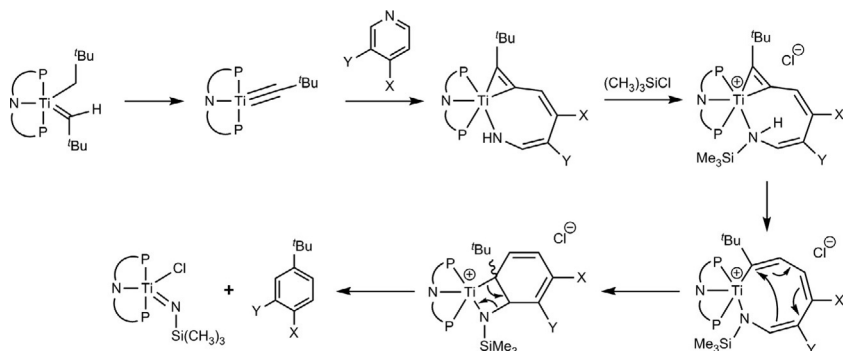
Scheme 11 Proposed mechanism for the denitrogenation of N-heterocycles.

titanium to form the intermediate **18C** which is located at −8.7 kcal/mol. Then, the well-matched charge distribution of Ti≡C and N═C leads to the formation of **18F** *via* bond metathesis with only 12.7 kcal/mol barrier. Finally, N—C bond cleavage occurs to generate intermediate **18G** and **18H** traversing additional rearrangement steps. Another plausible mechanism that was considered involves C—H activation of pyridine, and whereas the C—H activation step looks reasonable with transition state energy of 18.7 kcal/mol, the sequential steps were associated with too high energies to be mechanistically relevant. The η^2-(N,C) pyridyl complex **18D** was prepared experimentally using an independent route *via* direct transmetalation of $LiNC_5H_4$ with $(PNP)Ti$═$CH^tBu(OTf)$ at −100 °C to confirm the computational prediction that the C—H activation of pyridine is not a viable pathway, and thermolysis of η^2-(N,C) pyridyl complex did not produce the desired product **18H** (25 °C, 24 h). Despite the remarkable stability of this complex, addition of $(CH_3)_3SiCl$ as an electrophile over 72 h at 65 °C led to denitrogenation of N-heterocycle *via* several rearrangement steps as described in Scheme 11.[197]

3.5 Methane activation

The activation of the C—H bond in methane remains a difficult challenge[207] in general, and among the few possible strategies that can be envisioned for cleaving the C—H bond is designing a masked strong Brønsted base that can deprotonate methane. The difficulty of this approach stems from the fact that the pK_a of methane is ~50 and a classical deprotonation reaction is not likely to be successful. A more promising approach of utilizing the deprotonation route is offering a strong Brønsted base that is masked in

the sense that is revealed to the methane substrate only, while the formally anionic methyl moiety that is generated upon deprotonation is offered a strongly Lewis acidic binding partner, such that a significant amount of the energy that must be invested to cleave the strong C—H bond can be recovered. It is easy to see why this general strategy is practically impossible to implement, since the strong Brønsted base, which often tend to be strong Lewis bases, and the strong Lewis acid that are required within this reaction design will most likely react with each other, instead of reacting with methane that is an inert molecule for all practical purposes.

The aforementioned concerns point to a strategy of "masking" the Brønsted base/Lewis acidic characters in the reactive reagent. The titanium alkylidyne moiety is an intriguing candidate for this strategy. As we pointed out above, Schrock alkylidenes are already strong nucleophiles and can under certain circumstances act as strong Brønsted bases, as adding a proton to the alkylidene functionality will afford a stabile alkyl group. Similarly, the alkylidynes can be envisioned to be strong Brønsted bases and bind to a proton to give the corresponding alkylidene. Thus, several strategic consideration pointed to the titanium alkylidynes possibly being reactive toward methane. Both computational molecular modeling and experiments showed that this conceptual proposal is reasonable and the titanium alkylidyne complex was shown to activate methane at room temperature.[200] This result demonstrates the high reactivity of the Schrock carbyne moiety. The lessons learned from these studies have recently led to a very different, somewhat unrelated discovery of an unprecedentedly efficient catalytic borylation of methane using an Ir catalyst under relatively mild conditions.[208] Methane activation reactions remain difficult and often require much more forcing conditions.[209–211]

As shown in Fig. 19, the titanium–alkylidene system **19A** was obtained through the deprotonation of methane gas, in a mechanism that is analogous to what was found previously for the C—H activation of benzene and other alkane substrates. Fig. 19A shows the heterolytic C—H bond cleavage in methane by the highly nucleophilic carbon in the titanium alkylidyne complex, and Fig. 19B represents the two most probable reactions that complex **19A** may undergo, namely, tautomerization and C—H activation. The required barrier for the tautomerization was calculated to be 36 kcal/mol and tautomeric methylidene complex **19B** lies about 8 kcal/mol higher in energy, as shown in red in Fig. 19B. The optimized structures suggested an extremely weak α-agostic interaction of the methylidene, whereas a trigonal bipyramidal **19A–TSa** displayed an α-agostic interaction, which is believed to decrease the energy for tautomerization.
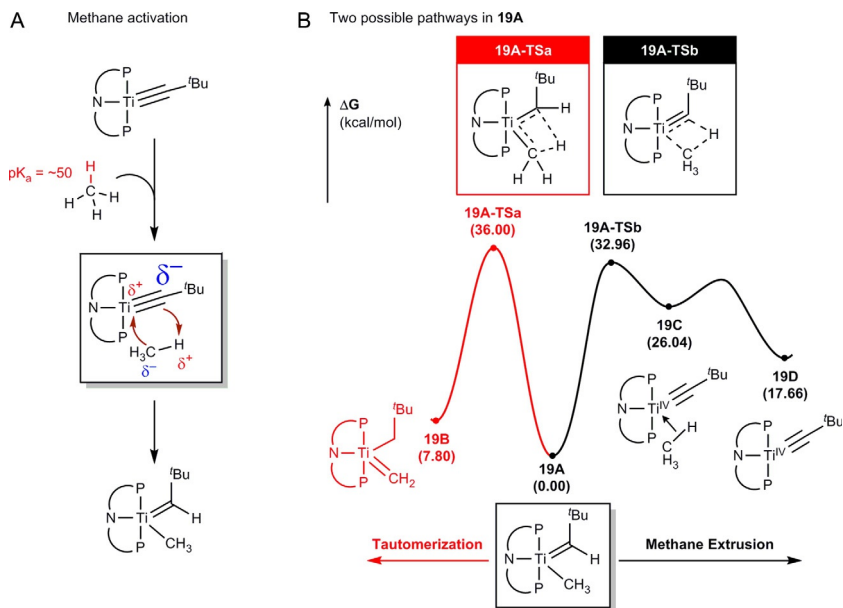
Fig. 19 (A) Methane activation *via* highly nucleophilic carbon of alkylidyne. (B) The computed energy profile for tautomerization and methane extrusion pathways in 19A remarked as red and black trace, respectively.

Recently, a unique transformation involving the intermediate **19A** was observed where methane is C—C coupled to ultimately give an olefin at room temperature[212], and a computational study revealed that the addition of a redox–active ligand such as thioxanthone or bipyridine enabled complex **19A** to undergo methyl migration pushing one electron onto the metal during that process to minimize the filled–filled interaction that would classically prevent the two Lewis basic fragments $[CH_3^-]$ and $[CH^tBu^{2-}]$ from approaching each other. Subsequent to the C—C bond formation, β–hydrogen abstraction or β–hydride elimination ultimately led to the olefination of methane.
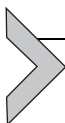
4. Computational studies on the Fischer type metathesis catalysts

4.1 Olefin metathesis using Fischer type catalysts

Even though the olefin metathesis using Schrock carbenes was studied in detail and the performance of catalysts based on Schrock carbenes were

superb, utilizing them as general purpose catalysts proved difficult, because they tend to be technically challenging to handle due to their being air sensitive, displaying relatively low functional group tolerance or simply being inconvenient to prepare. The Grubbs catalysts based on ruthenium carbene catalysts offer a solution to these practical issues and, consequently, they have been used much more broadly. In 1995, the first Ru-carbene olefin metathesis catalyst, $[Ru=CHPh(PR_3)_2Cl_2]$, was prepared.[213,214] These catalysts displayed significant advantages, such as being stable under air and showing high functional group tolerance. Unfortunately, the first generation of catalysts showed notably lower reactivities when compared to the Schrock type catalysts. Interestingly, the reactivity could be increased substantially in the second generation Grubbs catalysts by replacing the phosphine ligand with an NHC type ligand.[215] Further modifications on the ruthenium carbene catalysts suggested by Hoveyda enabled facile olefin metathesis reactions with high turnover numbers.[216,217]

Whereas the field of olefin metathesis catalysis reached a significant level of maturity, a few challenges have remained poorly met. The stereoselective synthesis of olefin products *via* olefin metathesis is one such challenge. Traditionally, the olefin metathesis reactions using Grubbs catalysts afforded minimal *E/Z*-selectivity due to the lack of steric hindrance between the NHC ligand and the olefin substrate. In 2011, Young and Fürstner developed (*E*)- or (*Z*)-selective ring-closing metathesis reactions using substrate control.[218,219] But this method limits the scope of substrate to silicon-containing alkenes, and is only applicable to macrocyclic ring-closing metathesis. Grubbs made a significant improvement on stereoselective olefin metathesis reactions, where a newly designed Ru catalyst containing an adamantyl group and a bidentate acetate ligand shows ∼90% selectivity for the (*Z*)-isomer.[220] Additional work provided catalysts with high levels of (*Z*)-selectivity[221] and the origin of the selectivity was understood by computational studies.[222]

These computational studies led to two major conclusions. The first concerns the orientation of the olefin approaching to the metal center. It was found that the olefin substrate can bind either to the bottom (*trans* to the NHC ligand) or to the side positions. DFT calculations with the simplest of olefins, ethylene, showed that there is an intrinsic electronic preference to adopt the side-bound geometry over the bottom-bound analogue. The initial insertion transition state of the side-bound mechanism shows an extremely low barrier of 4.1 kcal/mol, where the barrier of the insertion for the bottom-bound pathway was 16.9 kcal/mol. The strong preference

for the side-bound mechanism was explained with both steric and electronic effects. The chelating adamantyl group can cause large steric clashes with the alkylidene group and the olefin. As highlighted in Fig. 20B, the bottom-bound transition state shows the horizontal alignment of alkylidene and crashes with a bulky adamantyl group, whereas the alkylidene in the side-bound transition state can avoid the steric repulsion. Electronic effects also support the side-bound pathway. The insertion transition state of the side-bound pathway can have two distinctive π-backdonations, $d \rightarrow \pi^*$ (NHC) and $d \rightarrow \pi^*$ (alkylidene) to stabilize the structure. However, the analogous π-backdonations for the bottom-bound transition state involve the same Ru d orbital, which implies that each π-backdonation is weaker, resulting in smaller orbital interaction energy.

Following the optimized side-bound pathway, the stereoselectivity was investigated by explicitly considering the (E)- and (Z)-selective pathways. Fig. 21 illustrates the four different transition state structures of the the olefin metathesis step, where **32–TS** and **33–TS** correspond to the (Z)-selective pathway, while **34–TS** and **35–TS** show the (E)-selective pathway. As the NHC ligand contains two bulky substituents, an adamantyl group and a mesitylene group, their steric repulsions with olefin substrate destabilize the overall structure. From the optimized geometries, (E)-selective transition states showed significant steric repulsions between the methyl substituent and the bulky NHC ligand, while such unfavorable interaction is not present in the (Z)-selective case. This destabilization of **34–TS** and **35–TS** results in the prevention of (E)-selective olefin metathesis.

In addition to the Grubbs catalyst design, Hoveyda developed new catalysts for (Z)-selective olefin metathesis by introducing a bidentate catecholthiolate ligand.[223] The initial catalyst design was inspired by strategies to develop early transition metal catalysts for (Z)-selective olefin metathesis[112,224–226], which includes the control of steric repulsion to determine where the olefin approaches to the equatorial plane of the catalyst to afford high levels of (Z)-selectivity. As shown in Fig. 22, a dithiolate ligand was attached to the ruthenium center, and therefore one of the thiolates was forced to be positioned in the axial position of the NHC ligand. The dithiolate ligand was chosen because it can only bind in a *syn* alignment, whereas two chloride ligands in conventional Grubbs catalysts align *anti* orientation to each other. The newly designed (Z)-selective catalyst delivered high levels of stereoselectivity up to >98:2 in ring-opening metathesis[223] as well as in cross metathesis[213].
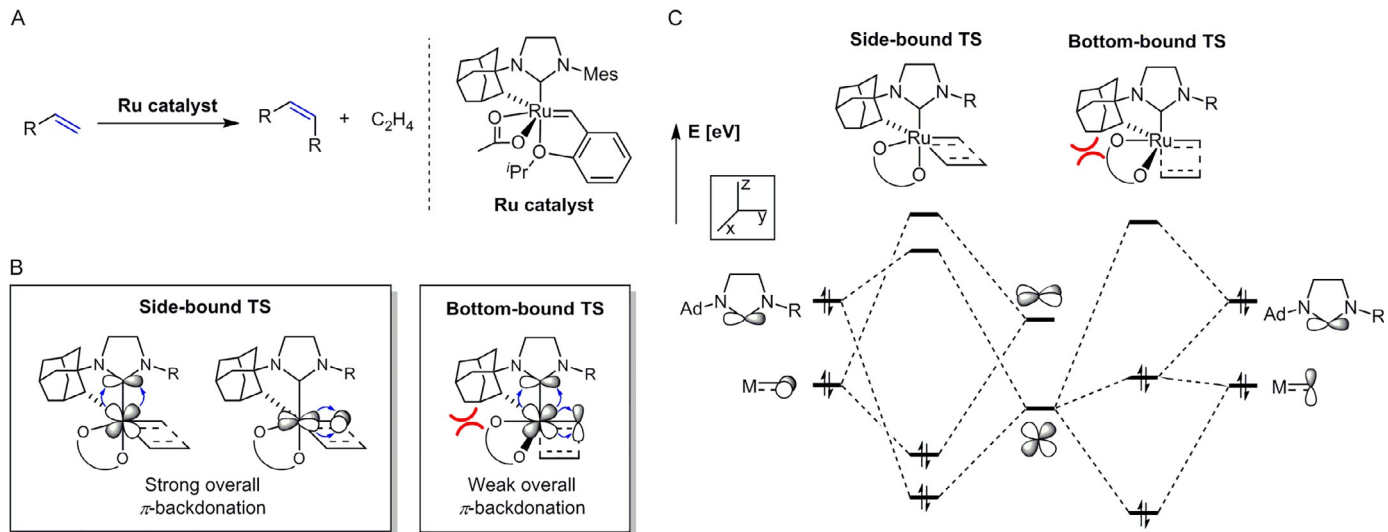
Fig. 20 (A) Schematic description for (Z)-selective olefin metathesis. (B and C) Molecular orbital diagram of the side-bound transition state (left) and the bottom-bound transition state (right) for the olefin insertion step.

Z-selective pathway

32-TS, $\Delta G^{\ddagger}$ = 14.6 kcal/mol   **33-TS**, $\Delta G^{\ddagger}$ = 14.4 kcal/mol

E-selective pathway

34-TS, $\Delta G^{\ddagger}$ = 16.1 kcal/mol   **35-TS**, $\Delta G^{\ddagger}$ = 18.8 kcal/mol
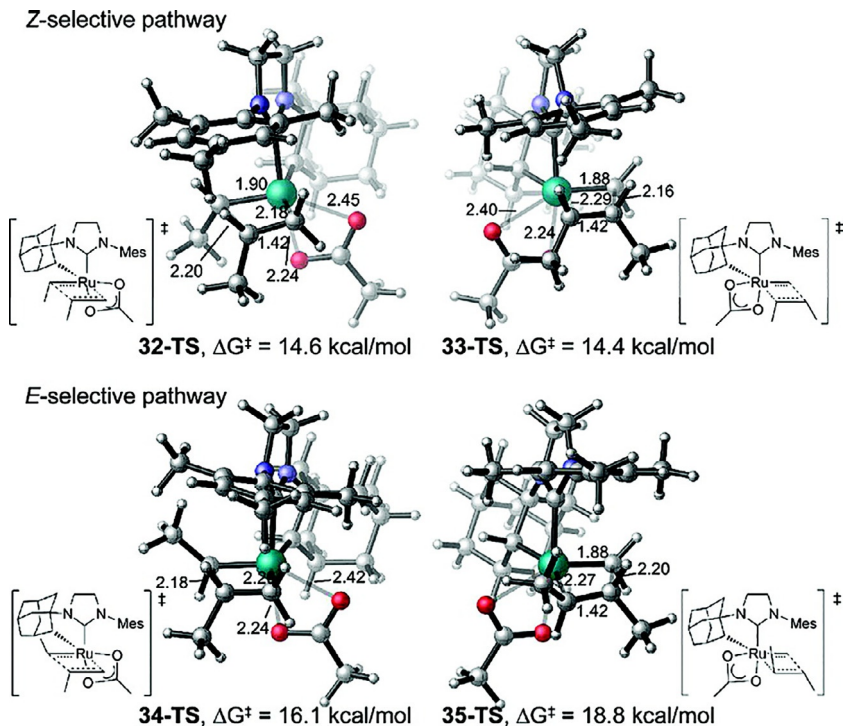
Fig. 21 Four different transition state structures of [2+2] cycloaddition step.[222] *Adapted from P. Liu, X. Xu, X. Dong, B. Keitz, M.B. Herbert, R.H. Grubbs, K.N. Houk, J. Am. Chem. Soc. 134 (2012) 1464–1467. Copyright 2012, American Chemical Society.*
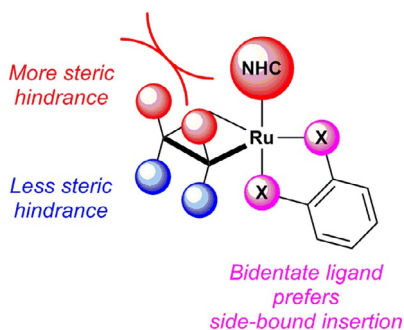
Fig. 22 Key structural features and elucidation for the design of (Z)-selective Ru catalysts.[223]

Computational studies highlighted the origin of high stereoselectivity of the Hoveyda (Z)-selective catalyst in the ring-opening metathesis.[227] Four possible approaches of olefin toward the metal center were evaluated by DFT calculations and the barrier of (Z)-selective pathway was found to be 3.2 kcal/mol at the insertion step, where it is only half of the barrier for the (E)-selective pathway. The unfavorable steric repulsion between the olefin substrate and the mesityl group attached to the NHC ligand is much more reduced for the (Z)-olefin formation pathway (Fig. 23).

An interesting feature of Hoveyda (Z)-selective catalyst is that it shows high *trans* selectivity in cross metathesis reactions through stereoretention, namely, the (Z)-olefins afford (Z)-olefin products while (E)-olefins convert to (E)-olefin products.[228] The origin for the highly stereoretentive olefin cross metathesis using a dithiolate catalyst was investigated computationally.[229] To test all possibilities, researchers took into account two major scenarios, just as was done in the other studies: bottom-bound and side-bound pathways, stressing that the initial binding location is critical for stereoselectivity. Based on the olefin insertion steps, stereoretention and stereoinversion cases were evaluated. As stated above, electronically, the side-bound pathway was much more preferred than the bottom-bound case, where the former is about 10 kcal/mol lower in energy than the latter typically. As illustrated in Fig. 24, steric repulsion between the NHC ligand and the substituents at α- and α'-positions must be minimized. Following this rule, the stereoretentive pathway is always favored over the stereoinversive case, where this rule is applicable to both E/Z-olefin formation.
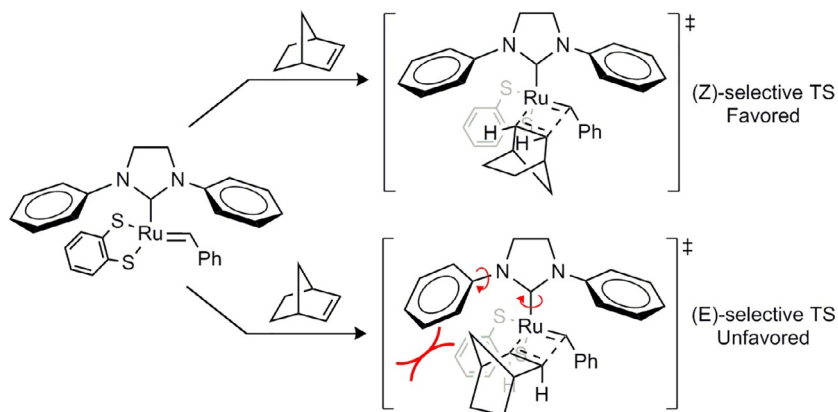
Fig. 23 Structural model of two transition states of Hoveyda (Z)-selective catalyst.
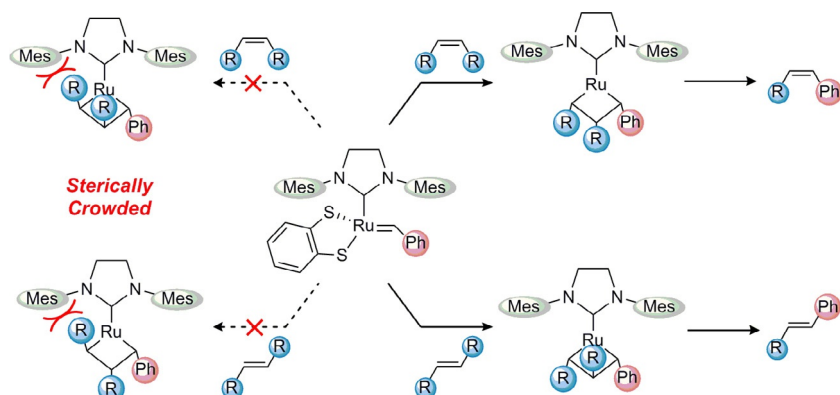
Fig. 24 Models for stereoretentive metathesis with (*Z*)-olefins (up) and (*E*)-olefins (down).[229]

4.2 Switching regioselectivity in cyclopolymerization of diynes using Ru[II]-alkylidene catalysts

Cyclopolymerization of terminal diynes is a powerful technique to synthesize conjugated polymers and these systems have been extensively studied using early transition metal catalysts including Ziegler type Ti catalysts[230,231], MoCl$_5$ and WCl$_6$.[232,233] But the first well–defined cyclopolymerization elucidating the structures of the prepared polymer as well as the mechanism was reported using Schrock type catalysts. Studies on cyclopolymerizations using Grubbs type olefin metathesis catalysts, however, were not known until Buchmeiser reported the first example.[234]

One of the most important features that is desirable to control in cyclopolymerization is the regioselectivity, which originates from the orientation of terminal alkynes to the Ru catalyst during the key C—C bond forming event. As described in Fig. 25, cyclopolymerization of diynes can produce two different regioisomers: five-membered conjugated rings *via* *α*-addition and six-membered rings by *β*-addition. These two different structural isomers are determined at the initial alkyne insertion step, as highlighted in Fig. 25. In a pioneering work by Schrock and Buchmeiser, it was shown that the regioselectivity control is possible with the Schrock type olefin metathesis catalysts. Unfortunately, the reason for the selectivity was not fully understood and the broad applicability remained somewhat limited due to the reasons mentioned above and difficulty in accessing the catalyst in sufficient quantities. Regrettably, stereoselective cyclopolymerization utilizing the Grubbs type catalysts that are easier to handle and are more easily accessible was not known.
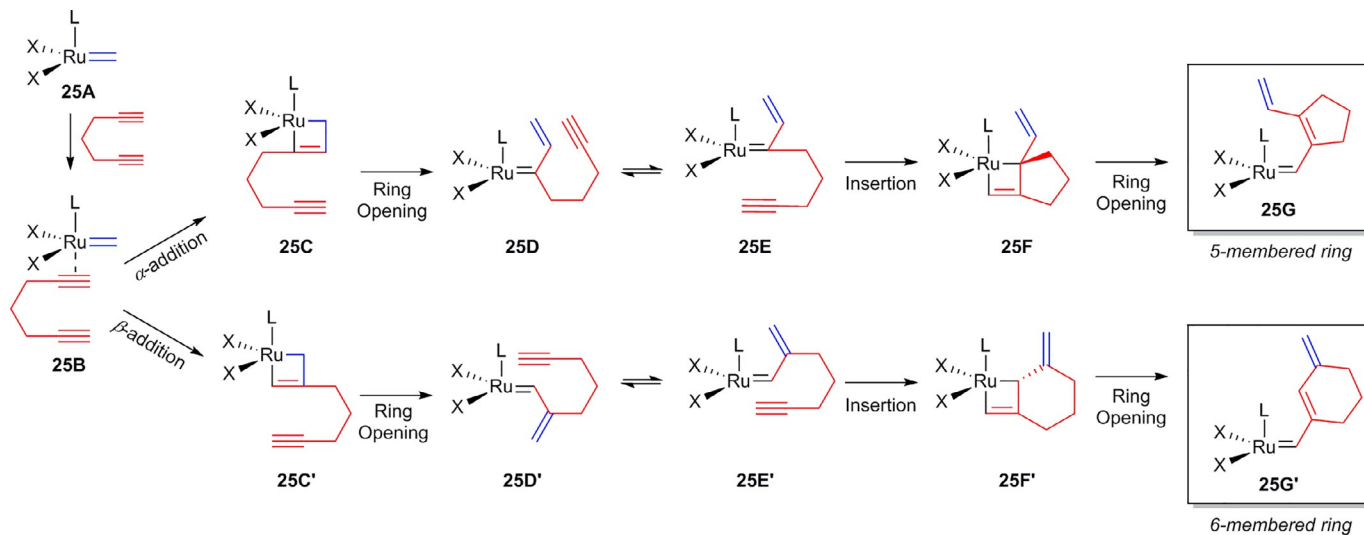
Fig. 25 Generalized illustration of the catalytic mechanisms of the Ru-catalyzed alkyne cyclopolymerization.[235]

Generally, the mechanism of cyclopolymerization involves the sequential insertion of the alkyne moiety followed by the ring-opening, as illustrated in Fig. 25. The diyne substrates can proceed in two distinctively different reaction channels at the initial stage of the reaction. After the reactant complex **25B** is formed, the alkyne substrate can undergo α–insertion to form the ruthenacyclobutene intermediate **25C**, followed by the ring-opening to give a ruthenium carbene intermediate **25D**. This ruthenium carbene intermediate can undergo a second alkyne insertion to produce the bicyclic ruthenacyclobutene intermediate **25F**. Final ring-opening furnishes the ruthenium complex carrying a carbene ligand that is tethered to the conjugated five-membered ring, which can reenter the catalytic cycle. If the initial alkyne insertion step occurs at the β-carbon, a six-membered ring intermediate is formed.

In 2011, Choi reported a highly α–selective cyclopolymerization of 1,6–heptadiyne utilizing the third-generation Grubbs catalyst (**Ru1** in Fig. 26)[236], and showed in a different example that living cyclopolymerization is also possible with a fast initiation by utilizing pyridine additives.[237] This work offered a solution for a long standing problem of cyclopolymerizing diynes in a highly β-selective way using ruthenium based catalysts. Choi also reported that the cyclopolymerization can be rendered (Z)-selective with certain Ru–catalysts (**Ru2**) bearing a sterically demanding adamantyl group and an NHC ligand, but the observed β-selectivity was limited to a range of 67–95% with **Ru2**.[238] To better understand the origin of the regioselectivity, computational studies using DFT calculations were carried out.[235]

The computed reaction energy diagrams for the initial insertion step with **Ru1**, **Ru2** catalysts are summarized in Fig. 26. In the **Ru1** system, the cyclopolymerization starts with the catalyst **26A** that subsequently forms **26B**, a reactive π-complex with the heptadiyne substrate at 10.4 kcal/mol. The two transition states, **26B–TS** and **26B–TS'** clearly show that the α-addition is more favorable than the β-addition by 9.2 kcal/mol. The following ruthenium carbene intermediates **26C** and **26D** are located at -15.7 and -8.1 kcal/mol, respectively, and imply that the initial insertion step is irreversible. On the contrary, the **Ru2** based cyclopolymerization predicts that the β-addition is more preferred over α-addition by 3.7 kcal/mol free energy difference. The insertion barriers of both pathways are extremely low with 7.6 and 3.9 kcal/mol, which is consistent with the observation that this reaction can be conducted at the low temperature condition. The full energy diagram of **Ru2** also supports the β-selectivity demand in cyclopolymerization.
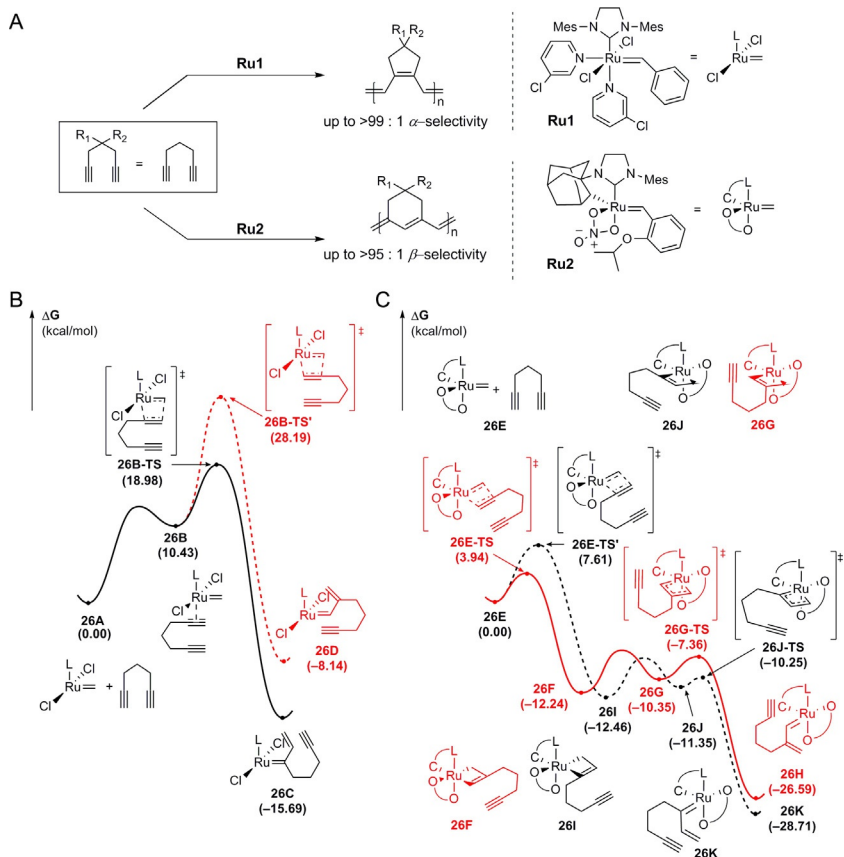
Fig. 26 (A) A summary from the experimental results and insertion step free energy diagram of the (B) **Ru1** system and the (C) **Ru2** system. $R_1 = R_2 = Et$ for the computational modeling study (black, α-addition; red, β-addition; plain, favored; dashed, disfavored; Refer ref. [235] for the detailed experimental conditions for cyclopolymerization).

Using the computational data in hand, the origin of regioselectivity in cyclopolymerization of diynes could be explained. Ruthenium carbene complexes are Fischer carbenes and have two major orbital interactions as we already discussed. Consequently, the catalyst-substrate alignment to successfully carry out α-addition is electronically preferred as the carbene carbon carries a partial positive charge while the terminal alkyne carbon is negatively charged, as summarized in Fig. 27A. The alignment to facilitate β-addition is not favorable because the partial charges of catalyst and substrate are mismatched. Steric effects can also be considered, as the **Ru2** catalyst prefers the side-bound mechanism, which is sterically favored for the β-addition to avoid the bulky mesityl group on the NHC ligand. Thus, both electronic
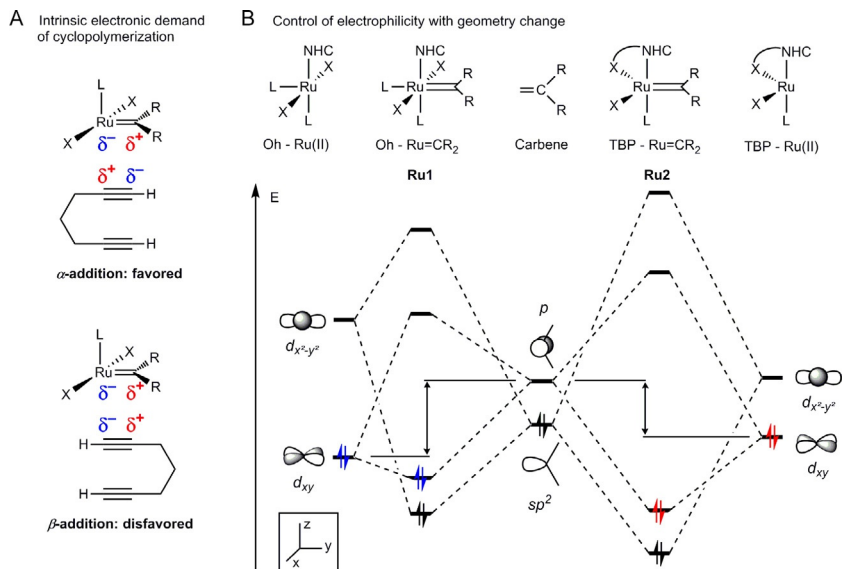
Fig. 27 (A) Intrinsic electronic demand of a typical Ru-Fischer carbene with a 1,6-heptadiyne substrate. (B) Qualitative molecular orbital diagram of carbene complexes.[235]

and steric effects point in the same energetic direction and add to afford the increased β-selectivity in **Ru2** catalytic system.

There are two slightly different structures for **Ru2** that are close enough in energy to establish a chemically meaningful equilibrium, namely, structures of pseudo–octahedral and trigonal bipyramidal coordination geometry due to the presence of the transient Ru—O bond. As explained in Fig. 27B, the structural change in ruthenium carbene complex gives rise to a change in electronic structure. The Ru-d_{xy} orbital energy level of the trigonal bipyramidal structure is higher than that of the octahedral geometry. On the other hand, the Ru-$d_{x^2-y^2}$ level in the trigonal bipyramidal structure is lower than that of the octahedral geometry. Therefore, the trigonal bipyramidal structure develops a stronger π-backbonding ability compared to the classical octahedral structure. This increased π-backdonation reduces the electrophilicity of the metal carbene complex and should show a different selectivity in cyclopolymerization as a result.

To test this concept, a new catalyst **Ru3**, a (Z)-selective olefin metathesis catalyst developed by Hoveyda[113,223], was tested (Fig. 28). Interestingly, the **Ru3** catalyst contains a rigid trigonal bipyramidal structure as the bidentate catecholthiolate ligand is forced to be arranged in a *syn* orientation
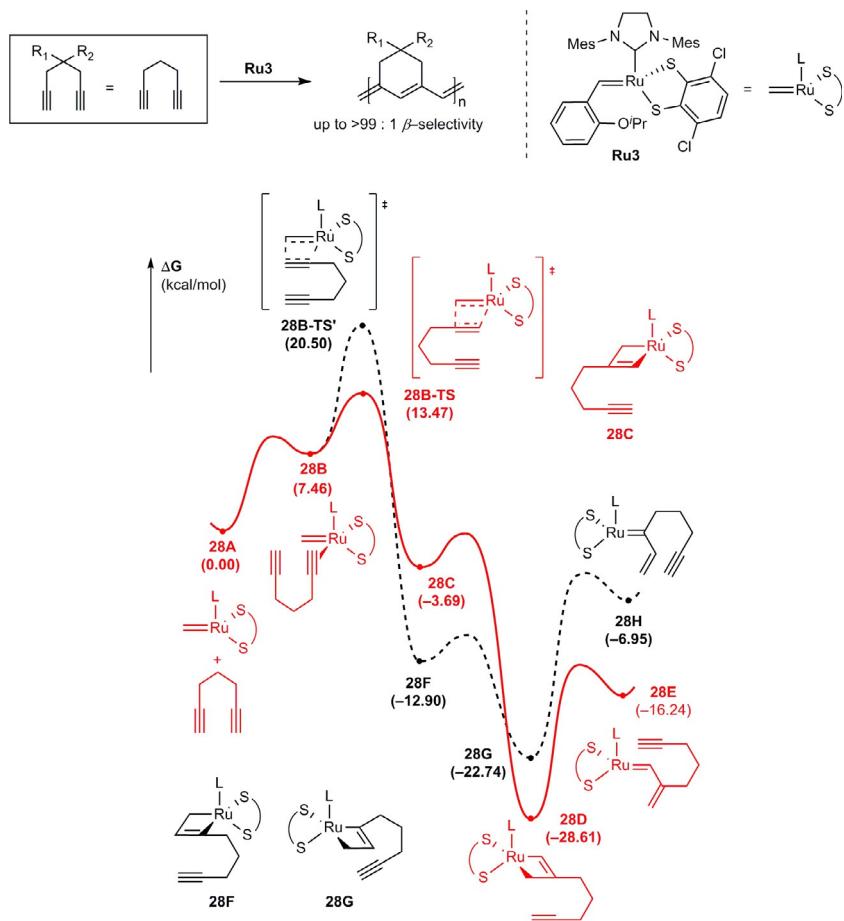
Fig. 28 Insertion step free energy diagram of the **Ru3** system and summarized experimental results. Refer ref. [235] for the detailed experimental condition. $R_1 = R_2 = Et$ for the computational modeling study (black, α-addition; red, β-addition; plain, favored; dashed, disfavored).

to each other. The computer simulation predicted that **Ru3** will prefer the β–addition over the α–addition by 7.0 kcal/mol free energy. Confirming the computational predictions, the experiments showed that the **Ru3** catalyst is highly β-selective and produced six–membered rings.

5. Conclusions and outlook

In this chapter, we summarized the progress that was made in under–standing and exploiting the unique features of the Schrock and Fischer

carbenes for a variety of chemical reactions. As the research field has matured over the last half century, the electronic structure difference of these two related, yet remarkably different classes of molecules has been delineated and computational methods played a major role in establishing a solid foundation of understanding of the electronic demand and the resulting reactivity. The olefin metathesis catalysis has been most dominating among catalytic applications and powerful catalysts could be developed using both Schrock and Fischer alkylidene complexes. The metal alkylidene motif has proven exceedingly useful for a variety of other challenging reactions, including C—H bond activation or pyridine ring-opening.

The alliance between computational and experimental work created an interesting platform of discovery that promises to expedite the development of new reactions. The alkylidene complexes have already revolutionized the olefin metathesis field, but the recent developments highlighted in this chapter show that this class of reactive molecules can be employed for many other purposes.

Acknowledgment

References

1. Schrock, R. R.; Czekelius, C. *Adv. Synth. Catal.* **2007**, *349*, 55–77.
2. Ogba, O. M.; Warner, N. C.; O'Leary, D. J.; Grubbs, R. H. *Chem. Soc. Rev.* **2018**, *47*, 4510–4544.
3. Fischer, E. O.; Maasböl, A. *Angew. Chem. Int. Ed. Eng.* **1964**, *3*, 580–581.
4. Schrock, R. R. *J. Am. Chem. Soc.* **1975**, *97*, 6577–6578.
5. Casey, C. P. *J. Chem. Educ.* **2006**, *83*, 192–195.
6. Grubbs, R. H. *Angew. Chem. Int. Ed.* **2006**, *45*, 3760–3765.
7. Schrock, R. R. *Angew. Chem. Int. Ed.* **2006**, *45*, 3748–3759.
8. Chauvin, Y. *Angew. Chem. Int. Ed.* **2006**, *45*, 3740–3747.
9. Chatt, J.; Duncanson, L. A.; Venanzi, L. M. *J. Chem. Soc.* **1955**, 4456–4460.
10. Chatt, J.; Duncanson, L. A. *J. Chem. Soc.* **1953**, 2939–2947.
11. Schrock, R. R. *J. Am. Chem. Soc.* **1974**, *96*, 6796–6797.
12. Fischer, E. O.; Maasböl, A. *Chem. Ber.* **1967**, *100*, 2445–2456.
13. Tebbe, F. N.; Parshall, G. W.; Reddy, G. S. *J. Am. Chem. Soc.* **1978**, *100*, 3611–3613.
14. Scott, J.; Mindiola, D. J. *Dalton Trans.* **2009**, 8463–8472.
15. Klabunde, U.; Tebbe, F. N.; Parshall, G. W.; Harlow, R. L. *J. Mol. Catal.* **1980**, *8*, 37–51.
16. Anslyn, E. V.; Grubbs, R. H. *J. Am. Chem. Soc.* **1987**, *109*, 4880–4890.
17. Gilliom, L. R.; Grubbs, R. H. *Organometallics* **1986**, *5*, 721–724.
18. Krusic, P. J.; Tebbe, F. N. *Inorg. Chem.* **1982**, *21*, 2900–2902.
19. Taylor, T. E.; Hall, M. B. *J. Am. Chem. Soc.* **1984**, *106*, 1576–1584.
20. Carter, E. A.; Goddard, W. A. *J. Am. Chem. Soc.* **1986**, *108*, 4746–4754.
21. Wu, Y.-D.; Peng, Z.-H.; Xue, Z. *J. Am. Chem. Soc.* **1996**, *118*, 9772–9777.
22. Kurogi, T.; Carroll, P. J.; Mindiola, D. J. *Chem. Commun.* **2017**, *53*, 3412–3414.

23. Grant, L. N.; Ahn, S.; Manor, B. C.; Baik, M.-H.; Mindiola, D. J. *Chem. Commun.* **2017**, *53*, 3415–3417.
24. Wiberg, K. B. *Tetrahedron* **1968**, *24*, 1083–1096.
25. Reed, A. E.; Weinhold, F. *J. Chem. Phys.* **1983**, *78*, 4066–4073.
26. Schwartz, J.; Gell, K. I. *J. Organomet. Chem.* **1980**, *184*, C1–C2.
27. von H. Spence, R. E.; Parks, D. J.; Piers, W. E.; MacDonald, M.-A.; Zaworotko, M. J.; Rettig, S. J. *Angew. Chem. Int. Ed. Engl.* **1995**, *34*, 1230–1233.
28. Thompson, R.; Nakamaru-Ogiso, E.; Chen, C.-H.; Pink, M.; Mindiola, D. J. *Organometallics* **2014**, *33*, 429–432.
29. Fryzuk, M. D.; Mao, S. S. H.; Zaworotko, M. J.; MacGillivray, L. R. *J. Am. Chem. Soc.* **1993**, *115*, 5336–5337.
30. Fryzuk, M. D.; Duval, P. B.; Mao, S. S. S. H.; Zaworotko, M. J.; MacGillivray, L. R. *J. Am. Chem. Soc.* **1999**, *121*, 2478–2487.
31. Fryzuk, M. D.; Duval, P. B.; Mao, S. S. S. H.; Rettig, S. J.; Zaworotko, M. J.; MacGillivray, L. R. *J. Am. Chem. Soc.* **1999**, *121*, 1707–1716.
32. Fryzuk, M. D.; Duval, P. B.; Patrick, B. O.; Rettig, S. J. *Organometallics* **2001**, *20*, 1608–1613.
33. Kamitani, M.; Pintér, B.; Chen, C.-H.; Pink, M.; Mindiola, D. J. *Angew. Chem. Int. Ed.* **2014**, *53*, 10913–10915.
34. Weng, W.; Yang, L.; Foxman, B. M.; Ozerov, O. V. *Organometallics* **2004**, *23*, 4700–4705.
35. Hessen, B.; Meetsma, A.; Teuben, J. H. *J. Am. Chem. Soc.* **1989**, *111*, 5977–5978.
36. Buijink, J.-K. F.; Teuben, J. H.; Kooijman, H.; Spek, A. L. *Organometallics* **1994**, *13*, 2922–2924.
37. Kilgore, U. J.; Sengelaub, C. A.; Fan, H. J.; Tomaszewski, J.; Karty, J. A.; Baik, M.-H.; Mindiola, D. J. *Organometallics* **2009**, *28*, 843–852.
38. Kilgore, U. J.; Fan, H.; Pink, M.; Urnezius, E.; Protasiewicz, J. D.; Mindiola, D. J. *Chem. Commun.* **2009**, 4521–4523.
39. Kilgore, U. J.; Sengelaub, C. A.; Pink, M.; Fout, A. R.; Mindiola, D. J. *Angew. Chem. Int. Ed.* **2008**, *47*, 3769–3772.
40. Basuli, F.; Bailey, B. C.; Brown, D.; Tomaszewski, J.; Huffman, J. C.; Baik, M.-H.; Mindiola, D. J. *J. Am. Chem. Soc.* **2004**, *126*, 10506–10507.
41. Basuli, F.; Kilgore, U. J.; Hu, X.; Meyer, K.; Pink, M.; Huffman, J. C.; Mindiola, D. J. *Angew. Chem. Int. Ed.* **2004**, *43*, 3156–3159.
42. Duncalf, D. J.; Harrison, R. J.; McCamley, A.; Royan, B. W. *J. Chem. Soc. Chem. Commun.* **1995**, 2421–2422.
43. Antinolo, A.; Otero, A.; Fajardo, M.; Garcia-Yebra, C.; Gil-Sanz, R.; Lopez-Mardomingo, C.; Martin, A.; Gomez-Sal, P. *Organometallics* **1994**, *13*, 4679–4682.
44. Antiñolo, A.; del Hierro, I.; Fajardo, M.; Garcia-Yuste, S.; Otero, A.; Blacque, O.; Kubicki, M. M.; Amaudrut, J. *Organometallics* **1996**, *15*, 1966–1971.
45. Searles, K.; Smith, K. T.; Kurogi, T.; Chen, C.-H.; Carroll, P. J.; Mindiola, D. J. *Angew. Chem. Int. Ed.* **2016**, *55*, 6642–6645.
46. Kilgore, U. J.; Tomaszewski, J.; Fan, H.; Huffman, J. C.; Mindiola, D. J. *Organometallics* **2007**, *26*, 6132–6138.
47. Kurogi, T.; Carroll, P. J.; Mindiola, D. J. *J. Am. Chem. Soc.* **2016**, *138*, 4306–4309.
48. VenkatRamani, S.; Roland, C. D.; Zhang, J. G.; Ghiviriga, I.; Abboud, K. A.; Veige, A. S. *Organometallics* **2016**, *35*, 2675–2682.
49. Chamberlain, L. R.; Rothwell, I. P.; Huffman, J. C. *J. Am. Chem. Soc.* **1986**, *108*, 1502–1509.
50. Chamberlain, L. R.; Rothwell, A. P.; Rothwell, I. P. *J. Am. Chem. Soc.* **1984**, *106*, 1847–1848.
51. Fryzuk, M. D.; Johnson, S. A.; Rettig, S. J. *Organometallics* **1999**, *18*, 4059–4067.

52. Gerber, L. C. H.; Watson, L. A.; Parkin, S.; Weng, W.; Foxman, B. M.; Ozerov, O. V. *Organometallics* **2007**, *26*, 4866–4868.
53. Chirik, P. J.; Zubris, D. L.; Ackerman, L. J.; Henling, L. M.; Day, M. W.; Bercaw, J. E. *Organometallics* **2003**, *22*, 172–187.
54. Antonelli, D. M.; Schaefer, W. P.; Parkin, G.; Bercaw, J. E. *J. Organomet. Chem.* **1993**, *462*, 213–220.
55. Sharp, P. R.; Schrock, R. R. *J. Organomet. Chem.* **1979**, *171*, 43–51.
56. Searles, K.; Pintér, B.; Chen, C.-H.; Mindiola, D. J. *Organometallics* **2014**, *33*, 4192–4199.
57. Dötz, K. H.; Stendel, J., Jr. *Chem. Rev.* **2009**, *109*, 3227–3274.
58. Coles, M. P.; Gibson, V. C.; Clegg, W.; Elsegood, M. R. J.; Porrelli, P. A. *Chem. Commun.* **1996**, 1963–1964.
59. Dötz, K. H.; Tomuschat, P. *Chem. Soc. Rev.* **1999**, *28*, 187–198.
60. Dötz, K. H. *Angew. Chem. Int. Ed. Eng.* **1975**, *14*, 644–645.
61. Wulff, W. D.; Tang, P. C.; McCallum, J. S. *J. Am. Chem. Soc.* **1981**, *103*, 7677–7678.
62. Sierra, M. A.; Mancheño, M. J.; Sáez, E.; del Amo, J. C. *J. Am. Chem. Soc.* **1998**, *120*, 6812–6813.
63. Wang, K.; Lu, Y.; Hu, F.; Yang, J.; Zhang, Y.; Wang, Z.-X.; Wang, J. *Organometallics* **2018**, *37*, 1–10.
64. Wang, K.; Wu, F.; Zhang, Y.; Wang, J. *Org. Lett.* **2017**, *19*, 2861–2864.
65. Schrock, R. R.; Murdzek, J. S.; Bazan, G. C.; Robbins, J.; DiMare, M.; O'Regan, M. *J. Am. Chem. Soc.* **1990**, *112*, 3875–3886.
66. Cundari, T. R.; Gordon, M. S. *Organometallics* **1992**, *11*, 55–63.
67. Fox, H. H.; Schofield, M. H.; Schrock, R. R. *Organometallics* **1994**, *13*, 2804–2815.
68. Poater, A.; Solans-Monfort, X.; Clot, E.; Copéret, C.; Eisenstein, O. *Dalton Trans.* **2006**, 3077–3087.
69. Solans-Monfort, X.; Eisenstein, O. *Polyhedron* **2006**, *25*, 339–348.
70. Cai, S.; Hoffman, D. M.; Wierda, D. A. *Organometallics* **1996**, *15*, 1023–1032.
71. Toreki, R.; Vaughan, G. A.; Schrock, R. R.; Davis, W. M. *J. Am. Chem. Soc.* **1993**, *115*, 127–137.
72. Chabanas, M.; Copéret, C.; Basset, J.-M. *Chem. Eur. J.* **2003**, *9*, 971–975.
73. Chabanas, M.; Baudouin, A.; Copéret, C.; Basset, J.-M. *J. Am. Chem. Soc.* **2001**, *123*, 2062–2063.
74. Copéret, C.; Chabanas, M.; Saint-Arroman, R. P.; Basset, J.-M. *Angew. Chem. Int. Ed.* **2003**, *42*, 156–181.
75. Solans-Monfort, X.; Clot, E.; Copéret, C.; Eisenstein, O. *Organometallics* **2005**, *24*, 1586–1597.
76. Green, M. L. H.; Hurley, C. R. *J. Organomet. Chem.* **1967**, *10*, 188–190.
77. Green, M. L. H.; Mitchard, L. C.; Swanwick, M. G. *J. Chem. Soc. A* **1971**, 794–797.
78. Riener, K.; Haslinger, S.; Raba, A.; Högerl, M. P.; Cokoja, M.; Herrmann, W. A.; Kühn, F. E. *Chem. Rev.* **2014**, *114*, 5215–5272.
79. Bedford, R. B.; Betham, M.; Bruce, D. W.; Danopoulos, A. A.; Frost, R. M.; Hird, M. *J. Org. Chem.* **2006**, *71*, 1104–1110.
80. Plietker, B. *Angew. Chem. Int. Ed.* **2006**, *45*, 1469–1473.
81. Pintauer, T.; Matyjaszewski, K. *Chem. Soc. Rev.* **2008**, *37*, 1087–1097.
82. Kandepi, V. V. K. M.; Cardoso, J. M. S.; Peris, E.; Royo, B. *Organometallics* **2010**, *29*, 2777–2782.
83. Nguyen, S. T.; Johnson, L. K.; Grubbs, R. H.; Ziller, J. W. *J. Am. Chem. Soc.* **1992**, *114*, 3974–3975.
84. Wulff, W. D.; Gilbertson, S. R.; Springer, J. P. *J. Am. Chem. Soc.* **1986**, *108*, 520–522.
85. Anderson, B. A.; Wulff, W. D.; Rheingold, A. L. *J. Am. Chem. Soc.* **1990**, *112*, 8615–8617.
86. Mo, Z.; Li, Y.; Lee, H. K.; Deng, L. *Organometallics* **2011**, *30*, 4687–4694.

87. Gao, K.; Yoshikai, N. *Acc. Chem. Res.* **2014**, *47*, 1208–1219.
88. Nakamura, E.; Yoshikai, N.; Yamanaka, M. *J. Am. Chem. Soc.* **2002**, *124*, 7181–7192.
89. Berry, J. F. *Dalton Trans.* **2012**, *41*, 700–713.
90. Pirrung, M. C.; Liu, H.; Morehead, A. T. *J. Am. Chem. Soc.* **2002**, *124*, 1014–1023.
91. Padwa, A.; Snyder, J. P.; Curtis, E. A.; Sheehan, S. M.; Worsencroft, K. J.; Kappe, C. O. *J. Am. Chem. Soc.* **2000**, *122*, 8155–8167.
92. Zalatan, D. N.; Du Bois, J. *J. Am. Chem. Soc.* **2008**, *130*, 9220–9221.
93. Hansen, J.; Autschbach, J.; Davies, H. M. L. *J. Org. Chem.* **2009**, *74*, 6555–6563.
94. Yoshikai, N.; Nakamura, E. *Adv. Synth. Catal.* **2003**, *345*, 1159–1171.
95. Cotton, F. A.; Curtis, N. F.; Harris, C. B.; Johnson, B. F. G.; Lippard, S. J.; Mague, J. T.; Robinson, W. R.; Wood, J. S. *Science* **1964**, *145*, 1305–1307.
96. Joost, M.; Estévez, L.; Mallet-Ladeira, S.; Miqueu, K.; Amgoune, A.; Bourissou, D. *Angew. Chem. Int. Ed.* **2014**, *53*, 14512–14516.
97. Harris, R. J.; Widenhoefer, R. A. *Angew. Chem. Int. Ed.* **2014**, *53*, 9369–9371.
98. Harris, R. J.; Widenhoefer, R. A. *Angew. Chem. Int. Ed.* **2015**, *54*, 6867–6869.
99. Joost, M.; Zeineddine, A.; Estévez, L.; Mallet-Ladeira, S.; Miqueu, K.; Amgoune, A.; Bourissou, D. *J. Am. Chem. Soc.* **2014**, *136*, 14654–14657.
100. Pujol, A.; Lafage, M.; Rekhroukh, F.; Saffon-Merceron, N.; Amgoune, A.; Bourissou, D.; Nebra, N.; Fustier-Boutignon, M.; Mézailles, N. *Angew. Chem. Int. Ed.* **2017**, *56*, 12264–12267.
101. Wilson, R. D.; Kamitori, Y.; Ogoshi, H.; Yoshida, Z.-I.; Ibers, J. A. *J. Organomet. Chem.* **1979**, *173*, 199–209.
102. Otsuka, S.; Nakamura, A.; Koyama, T.; Tatsuno, Y. *Justus Liebigs Ann. Chem.* **1975**, *1975*, 626–635.
103. Lappert, M. F.; Pye, P. L. *J. Chem. Soc., Dalton Trans.* **1977**, 2172–2180.
104. Arduengo, A. J.; Gamper, S. F.; Calabrese, J. C.; Davidson, F. *J. Am. Chem. Soc.* **1994**, *116*, 4391–4394.
105. Xia, Y.; Qiu, D.; Wang, J. *Chem. Rev.* **2017**, *117*, 13810–13889.
106. Premachandra, I. D. U. A.; Nguyen, T. A.; Shen, C.; Gutman, E. S.; Van Vranken, D. L. *Org. Lett.* **2015**, *17*, 5464–5467.
107. Zhao, X.; Wu, G.; Yan, C.; Lu, K.; Li, H.; Zhang, Y.; Wang, J. *Org. Lett.* **2010**, *12*, 5580–5583.
108. Mindiola, D. J.; Hillhouse, G. L. *J. Am. Chem. Soc.* **2002**, *124*, 9976–9977.
109. Harrold, N. D.; Waterman, R.; Hillhouse, G. L.; Cundari, T. R. *J. Am. Chem. Soc.* **2009**, *131*, 12872–12873.
110. Waterman, R.; Hillhouse, G. L. *J. Am. Chem. Soc.* **2003**, *125*, 13350–13351.
111. Iluc, V. M.; Hillhouse, G. L. *J. Am. Chem. Soc.* **2014**, *136*, 6479–6488.
112. Yu, M.; Wang, C.; Kyle, A. F.; Jakubec, P.; Dixon, D. J.; Schrock, R. R.; Hoveyda, A. H. *Nature* **2011**, *479*, 88–93.
113. Koh, M. J.; Khan, R. K. M.; Torker, S.; Yu, M.; Mikus, M. S.; Hoveyda, A. H. *Nature* **2015**, *517*, 181–186.
114. Kress, S.; Blechert, S. *Chem. Soc. Rev.* **2012**, *41*, 4389–4408.
115. Hoveyda, A. H.; Zhugralin, A. R. *Nature* **2007**, *450*, 243–251.
116. Jean-Louis Hérisson, P.; Chauvin, Y. *Makromol. Chem.* **1971**, *141*, 161–176.
117. Woodward, R. B.; Hoffmann, R. *J. Am. Chem. Soc.* **1965**, *87*, 395–397.
118. Schrock, R. R. *Tetrahedron* **1999**, *55*, 8141–8153.
119. Schrock, R. R.; Hoveyda, A. H. *Angew. Chem. Int. Ed.* **2003**, *42*, 4592–4633.
120. Oskam, J. H.; Schrock, R. R. *J. Am. Chem. Soc.* **1993**, *115*, 11831–11845.
121. Feldman, J.; Davis, W. M.; Thomas, J. K.; Schrock, R. R. *Organometallics* **1990**, *9*, 2535–2548.
122. Love, J. A.; Sanford, M. S.; Day, M. W.; Grubbs, R. H. *J. Am. Chem. Soc.* **2003**, *125*, 10103–10109.

123. Sanford, M. S.; Love, J. A.; Grubbs, R. H. *J. Am. Chem. Soc.* **2001**, *123*, 6543–6554.
124. Sanford, M. S.; Ulman, M.; Grubbs, R. H. *J. Am. Chem. Soc.* **2001**, *123*, 749–750.
125. Dias, E. L.; Nguyen, S. T.; Grubbs, R. H. *J. Am. Chem. Soc.* **1997**, *119*, 3887–3897.
126. Ulman, M.; Grubbs, R. H. *Organometallics* **1998**, *17*, 2484–2489.
127. Grubbs, R. H.; Chang, S. *Tetrahedron* **1998**, *54*, 4413–4450.
128. Trnka, T. M.; Grubbs, R. H. *Acc. Chem. Res.* **2001**, *34*, 18–29.
129. Folga, E.; Ziegler, T. *Organometallics* **1993**, *12*, 325–337.
130. Monteyne, K.; Ziegler, T. *Organometallics* **1998**, *17*, 5901–5907.
131. Wu, Y.-D.; Peng, Z.-H. *J. Am. Chem. Soc.* **1997**, *119*, 8043–8049.
132. Aagaard, O. M.; Meier, R. J.; Buda, F. *J. Am. Chem. Soc.* **1998**, *120*, 7174–7182.
133. Weskamp, T.; Kohl, F. J.; Hieringer, W.; Gleich, D.; Herrmann, W. A. *Angew. Chem. Int. Ed.* **1999**, *38*, 2416–2419.
134. Adlhart, C.; Hinderling, C.; Baumann, H.; Chen, P. *J. Am. Chem. Soc.* **2000**, *122*, 8204–8214.
135. Cavallo, L. *J. Am. Chem. Soc.* **2002**, *124*, 8965–8973.
136. Adlhart, C.; Chen, P. *Angew. Chem. Int. Ed.* **2002**, *41*, 4484–4487.
137. Vyboishchikov, S. E.; Bühl, M.; Thiel, W. *Chem. Eur. J.* **2002**, *8*, 3962–3975.
138. Fomine, S.; Vargas, S. M.; Tlenkopatchev, M. A. *Organometallics* **2003**, *22*, 93–99.
139. Adlhart, C.; Chen, P. *J. Am. Chem. Soc.* **2004**, *126*, 3496–3510.
140. Eisenstein, O.; Hoffmann, R.; Rossi, A. R. *J. Am. Chem. Soc.* **1981**, *103*, 5582–5584.
141. Hoveyda, A. H. *J. Org. Chem.* **2014**, *79*, 4763–4792.
142. Werrel, S.; Walker, J. C. L.; Donohoe, T. J. *Tetrahedron Lett.* **2015**, *56*, 5261–5268.
143. du Toit, J. I.; van Sittert, C. G. C. E.; Vosloo, H. C. M. *J. Organomet. Chem.* **2013**, *738*, 76–91.
144. Schrock, R. R.; DePue, R. T.; Feldman, J.; Schaverien, C. J.; Dewan, J. C.; Liu, A. H. *J. Am. Chem. Soc.* **1988**, *110*, 1423–1435.
145. Murdzek, J. S.; Schrock, R. R. *Organometallics* **1987**, *6*, 1373–1374.
146. Oskam, J. H.; Fox, H. H.; Yap, K. B.; McConville, D. H.; O'Dell, R.; Lichtenstein, B. J.; Schrock, R. R. *J. Organomet. Chem.* **1993**, *459*, 185–198.
147. Alexander, J. B.; Schrock, R. R.; Davis, W. M.; Hultzsch, K. C.; Hoveyda, A. H.; Houser, J. H. *Organometallics* **2000**, *19*, 3700–3715.
148. Aeilts, S. L.; Cefalo, D. R.; Bonitatebus, J.; Peter, J.; Houser, J. H.; Hoveyda, A. H.; Schrock, R. R. *Angew. Chem. Int. Ed.* **2001**, *40*, 1452–1456.
149. Singh, R.; Schrock, R. R.; Müller, P.; Hoveyda, A. H. *J. Am. Chem. Soc.* **2007**, *129*, 12654–12655.
150. Sattely, E. S.; Meek, S. J.; Malcolmson, S. J.; Schrock, R. R.; Hoveyda, A. H. *J. Am. Chem. Soc.* **2009**, *131*, 943–953.
151. Amatore, C.; Jutand, A.; M'Barki, M. A. *Organometallics* **1992**, *11*, 3009–3013.
152. Solans-Monfort, X.; Clot, E.; Copéret, C.; Eisenstein, O. *J. Am. Chem. Soc.* **2005**, *127*, 14015–14025.
153. Goumans, T. P. M.; Ehlers, A. W.; Lammertsma, K. *Organometallics* **2005**, *24*, 3200–3206.
154. Crowe, W. E.; Zhang, Z. J. *J. Am. Chem. Soc.* **1993**, *115*, 10998–10999.
155. Meek, S. J.; Malcolmson, S. J.; Li, B.; Schrock, R. R.; Hoveyda, A. H. *J. Am. Chem. Soc.* **2009**, *131*, 16407–16409.
156. Hoveyda, A. H.; Schrock, R. R. *Chem. Eur. J.* **2001**, *7*, 945–950.
157. Poater, A.; Solans-Monfort, X.; Clot, E.; Copéret, C.; Eisenstein, O. *J. Am. Chem. Soc.* **2007**, *129*, 8207–8216.
158. Leduc, A.-M.; Salameh, A.; Soulivong, D.; Chabanas, M.; Basset, J.-M.; Copéret, C.; Solans-Monfort, X.; Clot, E.; Eisenstein, O.; Böhm, V. P. W.; Röper, M. *J. Am. Chem. Soc.* **2008**, *130*, 6288–6297.
159. Vasiliu, M.; Li, S.; Arduengo, A. J., III; Dixon, D. A. *J. Phys. Chem. C* **2011**, *115*, 12106–12120.

160. Solans-Monfort, X.; Copéret, C.; Eisenstein, O. *Organometallics* **2012**, *31*, 6812–6822.
161. Solans-Monfort, X.; Copéret, C.; Eisenstein, O. *Organometallics* **2015**, *34*, 1668–1680.
162. Marinescu, S. C.; Schrock, R. R.; Müller, P.; Hoveyda, A. H. *J. Am. Chem. Soc.* **2009**, *131*, 10840–10841.
163. Nasr, A.; Breuil, P.-A. R.; Silva, D. C.; Berthod, M.; Dellus, N.; Jeanneau, E.; Lemaire, M.; Olivier-Bourbigou, H. *Organometallics* **2013**, *32*, 5320–5325.
164. Rendón, N.; Berthoud, R.; Blanc, F.; Gajan, D.; Maishal, T.; Basset, J.-M.; Copéret, C.; Lesage, A.; Emsley, L.; Marinescu, S. C.; Singh, R.; Schrock, R. R. *Chem. Eur. J.* **2009**, *15*, 5083–5089.
165. Mougel, V.; Pucino, M.; Copéret, C. *Organometallics* **2015**, *34*, 551–554.
166. Balcells, D.; Clot, E.; Eisenstein, O. *Chem. Rev.* **2010**, *110*, 749–823.
167. Whited, M. T.; Grubbs, R. H. *Acc. Chem. Res.* **2009**, *42*, 1607–1616.
168. van der Heijden, H.; Hessen, B. *J. Chem. Soc. Chem. Commun.* **1995**, 145–146.
169. Adams, C. S.; Legzdins, P.; Tran, E. *J. Am. Chem. Soc.* **2001**, *123*, 612–624.
170. Adams, C. S.; Legzdins, P.; McNeil, W. S. *Organometallics* **2001**, *20*, 4939–4955.
171. Adams, C. S.; Legzdins, P.; Tran, E. *Organometallics* **2002**, *21*, 1474–1486.
172. Andino, J. G.; Kilgore, U. J.; Pink, M.; Ozarowski, A.; Krzystek, J.; Telser, J.; Baik, M.-H.; Mindiola, D. J. *Chem. Sci.* **2010**, *1*, 351–356.
173. Fischer, E. O.; Kreis, G.; Kreiter, C. G.; Müller, J.; Huttner, G.; Lorenz, H. *Angew. Chem. Int. Ed. Eng.* **1973**, *12*, 564–565.
174. Protasiewicz, J. D.; Lippard, S. J. *J. Am. Chem. Soc.* **1991**, *113*, 6564–6570.
175. Schrock, R. R. *Chimia* **2015**, *69*, 388–392.
176. Yang, H.; Jin, Y.; Du, Y.; Zhang, W. *J. Mater. Chem. A* **2014**, *2*, 5986–5993.
177. Fürstner, A. *Angew. Chem. Int. Ed.* **2013**, *52*, 2794–2819.
178. Wu, X.; Tamm, M. *Beilstein J. Org. Chem.* **2011**, *7*, 82–93.
179. Schrock, R. R. *Chem. Commun.* **2013**, *49*, 5529–5531.
180. Hill, A. F.; Ward, J. S.; Xiong, Y. *Organometallics* **2015**, *34*, 5057–5064.
181. Filippou, A. C.; Lungwitz, B.; Wanninger, K. M. A.; Herdtweck, E. *Angew. Chem. Int. Ed. Eng.* **1995**, *34*, 924–927.
182. Manna, J.; Kuk, R. J.; Dallinger, R. F.; Hopkins, M. D. *J. Am. Chem. Soc.* **1994**, *116*, 9793–9794.
183. Beer, S.; Brandhorst, K.; Hrib, C. G.; Wu, X.; Haberlag, B.; Grunenberg, J.; Jones, P. G.; Tamm, M. *Organometallics* **2009**, *28*, 1534–1545.
184. Wengrovius, J. H.; Sancho, J.; Schrock, R. R. *J. Am. Chem. Soc.* **1981**, *103*, 3932–3934.
185. Du, Y.; Yang, H.; Zhu, C.; Ortiz, M.; Okochi, K. D.; Shoemaker, R.; Jin, Y.; Zhang, W. *Chem. Eur. J.* **2016**, *22*, 7959–7963.
186. von Kugelgen, S.; Bellone, D. E.; Cloke, R. R.; Perkins, W. S.; Fischer, F. R. *J. Am. Chem. Soc.* **2016**, *138*, 6234–6239.
187. Cromm, P. M.; Schaubach, S.; Spiegel, J.; Fürstner, A.; Grossmann, T. N.; Waldmann, H. *Nat. Commun.* **2016**, *7*, 11300.
188. Guo, L.-D.; Huang, X.-Z.; Luo, S.-P.; Cao, W.-S.; Ruan, Y.-P.; Ye, J.-L.; Huang, P.-Q. *Angew. Chem. Int. Ed.* **2016**, *55*, 4064–4068.
189. Lee, S.; Yang, A.; Moneypenny, T. P.; Moore, J. S. *J. Am. Chem. Soc.* **2016**, *138*, 2182–2185.
190. Wang, Q.; Yu, C.; Zhang, C.; Long, H.; Azarnoush, S.; Jin, Y.; Zhang, W. *Chem. Sci.* **2016**, *7*, 3370–3376.
191. Schaubach, S.; Gebauer, K.; Ungeheuer, F.; Hoffmeister, L.; Ilg, M. K.; Wirtz, C.; Fürstner, A. *Chem. Eur. J.* **2016**, *22*, 8494–8507.
192. Bailey, B. C.; Fan, H.; Baum, E. W.; Huffman, J. C.; Baik, M.-H.; Mindiola, D. J. *J. Am. Chem. Soc.* **2005**, *127*, 16016–16017.
193. Bailey, B. C.; Fan, H.; Huffman, J. C.; Baik, M.-H.; Mindiola, D. J. *J. Am. Chem. Soc.* **2007**, *129*, 8781–8793.

194. Bailey, B. C.; Huffman, J. C.; Mindiola, D. J.; Weng, W.; Ozerov, O. V. *Organometallics* **2005**, *24*, 1390–1393.
195. Bailey, B. C.; Huffman, J. C.; Mindiola, D. J. *J. Am. Chem. Soc.* **2007**, *129*, 5302–5303.
196. Bailey, B. C.; Fan, H.; Huffman, J. C.; Baik, M.-H.; Mindiola, D. J. *J. Am. Chem. Soc.* **2006**, *128*, 6798–6799.
197. Fout, A. R.; Bailey, B. C.; Tomaszewski, J.; Mindiola, D. J. *J. Am. Chem. Soc.* **2007**, *129*, 12640–12641.
198. Cavaliere, V. N.; Crestani, M. G.; Pintér, B.; Pink, M.; Chen, C. H.; Baik, M.-H.; Mindiola, D. J. *J. Am. Chem. Soc.* **2011**, *133*, 10700–10703.
199. Crestani, M. G.; Hickey, A. K.; Gao, X.; Pinter, B.; Cavaliere, V. N.; Ito, J.-I.; Chen, C.-H.; Mindiola, D. J. *J. Am. Chem. Soc.* **2013**, *135*, 14754–14767.
200. Flores, J. A.; Cavaliere, V. N.; Buck, D.; Pintér, B.; Chen, G.; Crestani, M. G.; Baik, M.–H.; Mindiola, D. J. *Chem. Sci.* **2011**, *2*, 1457–1462.
201. Goldman, A. S.; Roy, A. H.; Huang, Z.; Ahuja, R.; Schinski, W.; Brookhart, M. *Science* **2006**, *312*, 257–261.
202. Solowey, D. P.; Mane, M. V.; Kurogi, T.; Carroll, P. J.; Manor, B. C.; Baik, M.-H.; Mindiola, D. J. *Nat. Chem.* **2017**, *9*, 1126–1132.
203. Kleckley, T. S.; Bennett, J. L.; Wolczanski, P. T.; Lobkovsky, E. B. *J. Am. Chem. Soc.* **1997**, *119*, 247–248.
204. Strickler, J. R.; Bruck, M. A.; Wigley, D. E. *J. Am. Chem. Soc.* **1990**, *112*, 2814–2816.
205. Gray, S. D.; Weller, K. J.; Bruck, M. A.; Briggs, P. M.; Wigley, D. E. *J. Am. Chem. Soc.* **1995**, *117*, 10678–10693.
206. Gray, S. D.; Smith, D. P.; Bruck, M. A.; Wigley, D. E. *J. Am. Chem. Soc.* **1992**, *114*, 5462–5463.
207. Cavaliere, V. N.; Mindiola, D. *J. Chem. Sci.* **2012**, *3*, 3356–3365.
208. Smith, K. T.; Berritt, S.; González-Moreiras, M.; Ahn, S.; Smith, M. R.; Baik, M.-H.; Mindiola, D. J. *Science* **2016**, *351*, 1424–1427.
209. Cook, A. K.; Schimler, S. D.; Matzger, A. J.; Sanford, M. S. *Science* **2016**, *351*, 1421–1424.
210. Jones, C.; Taube, D.; Ziatdinov, V. R.; Periana, R. A.; Nielsen, R. J.; Oxgaard, J.; Goddard, W. A. *Angew. Chem.* **2004**, *116*, 4726–4729.
211. Caballero, A.; Pérez, P. J. *Chem. Soc. Rev.* **2013**, *42*, 8809–8820.
212. Kurogi, T.; Won, J.; Park, B.; Trofymchuk, O. S.; Carroll, P. J.; Baik, M.-H.; Mindiola, D. J. *Chem. Sci.* **2018**, *9*, 3376–3385.
213. Schwab, P.; France, M. B.; Ziller, J. W.; Grubbs, R. H. *Angew. Chem. Int. Ed. Eng.* **1995**, *34*, 2039–2041.
214. Schwab, P.; Grubbs, R. H.; Ziller, J. W. *J. Am. Chem. Soc.* **1996**, *118*, 100–110.
215. Scholl, M.; Trnka, T. M.; Morgan, J. P.; Grubbs, R. H. *Tetrahedron Lett.* **1999**, *40*, 2247–2250.
216. Kingsbury, J. S.; Harrity, J. P. A.; Bonitatebus, P. J.; Hoveyda, A. H. *J. Am. Chem. Soc.* **1999**, *121*, 791–799.
217. Garber, S. B.; Kingsbury, J. S.; Gray, B. L.; Hoveyda, A. H. *J. Am. Chem. Soc.* **2000**, *122*, 8168–8179.
218. Wang, Y.; Jimenez, M.; Hansen, A. S.; Raiber, E.-A.; Schreiber, S. L.; Young, D. W. *J. Am. Chem. Soc.* **2011**, *133*, 9196–9199.
219. Gallenkamp, D.; Fürstner, A. *J. Am. Chem. Soc.* **2011**, *133*, 9232–9235.
220. Endo, K.; Grubbs, R. H. *J. Am. Chem. Soc.* **2011**, *133*, 8525–8527.
221. Keitz, B. K.; Endo, K.; Patel, P. R.; Herbert, M. B.; Grubbs, R. H. *J. Am. Chem. Soc.* **2012**, *134*, 693–699.
222. Liu, P.; Xu, X.; Dong, X.; Keitz, B. K.; Herbert, M. B.; Grubbs, R. H.; Houk, K. N. *J. Am. Chem. Soc.* **2012**, *134*, 1464–1467.

223. Khan, R. K. M.; Torker, S.; Hoveyda, A. H. *J. Am. Chem. Soc.* **2013**, *135*, 10258–10261.
224. Ibrahem, I.; Yu, M.; Schrock, R. R.; Hoveyda, A. H. *J. Am. Chem. Soc.* **2009**, *131*, 3844–3845.
225. Flook, M. M.; Jiang, A. J.; Schrock, R. R.; Müller, P.; Hoveyda, A. H. *J. Am. Chem. Soc.* **2009**, *131*, 7962–7963.
226. Meek, S. J.; O'Brien, R. V.; Llaveria, J.; Schrock, R. R.; Hoveyda, A. H. *Nature* **2011**, *471*, 461–466.
227. Xu, C.; Liu, Z.; Torker, S.; Shen, X.; Xu, D.; Hoveyda, A. H. *J. Am. Chem. Soc.* **2017**, *139*, 15640–15643.
228. Johns, A. M.; Ahmed, T. S.; Jackson, B. W.; Grubbs, R. H.; Pederson, R. L. *Org. Lett.* **2016**, *18*, 772–775.
229. Grandner, J. M.; Shao, H.; Grubbs, R. H.; Liu, P.; Houk, K. N. *J. Org. Chem.* **2017**, *82*, 10595–10600.
230. Gibson, H. W.; Epstein, A. J.; Rommelmann, H.; Tanner, D. B.; Yang, X.-Q.; Pochan, J. M. *J. Phys. Colloq.* **1983**, *44*, C3-651–C3-656.
231. Gibson, H. W.; Bailey, F. C.; Epstein, A. J.; Rommelmann, H.; Kaplan, S.; Harbour, J.; Yang, X. Q.; Tanner, D. B.; Pochan, J. M. *J. Am. Chem. Soc.* **1983**, *105*, 4417–4431.
232. Jang, M. S.; Kwon, S. K.; Choi, S. K. *Macromolecules* **1990**, *23*, 4135–4140.
233. Koo, K. M.; Han, S. H.; Kang, Y. S.; Kim, U. Y.; Choi, S. K. *Macromolecules* **1993**, *26*, 2485–2488.
234. Krause, J. O.; Zarka, M. T.; Anders, U.; Weberskirch, R.; Nuyken, O.; Buchmeiser, M. R. *Angew. Chem. Int. Ed.* **2003**, *42*, 5965–5969.
235. Jung, H.; Jung, K.; Hong, M.; Kwon, S.; Kim, K.; Hong, S. H.; Choi, T.-L.; Baik, M.-H. *J. Am. Chem. Soc.* **2018**, *140*, 834–841.
236. Kang, E.-H.; Lee, I. S.; Choi, T.-L. *J. Am. Chem. Soc.* **2011**, *133*, 11904–11907.
237. Kang, E.-H.; Yu, S. Y.; Lee, I. S.; Park, S. E.; Choi, T.-L. *J. Am. Chem. Soc.* **2014**, *136*, 10508–10514.
238. Jung, K.; Kang, E.-H.; Sohn, J.-H.; Choi, T.-L. *J. Am. Chem. Soc.* **2016**, *138*, 11227–11233.